ACS APPLIED MATERIALS & INTERFACES

www.acsami.org

Research Article

Two-Dimensional Metal–Organic Framework with Ultrahigh Water Stability for Separation of Acetylene from Carbon Dioxide and Ethylene

Shan-Qing Yang, Lei Zhou, Yabing He, Rajamani Krishna, Qiang Zhang, Yi-Feng An, Bo Xing, Ying-Hui Zhang, and Tong-Liang Hu*

Cite This: *ACS Appl. Mater. Interfaces* 2022, 14, 33429–33437

Read Online

ACCESS | Metrics & More | Article Recommendations | Supporting Information

ABSTRACT: Highly selective separation and purification of acetylene (C_2H_2) from ethylene (C_2H_4) and carbon dioxide (CO_2) are daunting challenges in light of their similar molecule sizes and physical properties. Herein, we report a two-dimensional (2D) stable metal–organic framework (MOF), **NUM-11** ([Cu-(Hmpba)$_2$]·1.5DMF) (H_2mpba = 4-(3,5-dimethyl-1*H*-pyrazol-4-yl)benzoic acid), with *sql* topology, stacked together through $\pi-\pi$ interactions for efficient separation of C_2H_2 from C_2H_4 and CO_2. The 2D-MOF material offers high hydrolytic stability and good purification capacity; especially, it could survive in water for 7 months, even longer. This stable MOF selectively captures C_2H_2 from mixtures containing C_2H_4 and CO_2, as determined by adsorption isotherms. The ideal adsorbed solution theory selectivity calculations and transient breakthrough experiments were performed to verify the separation capacity. The low isosteric heat of **NUM-11a** (desolvated **NUM-11**) (18.24 kJ mol^{-1} for C_2H_2) validates the feasibility of adsorbent regeneration with low energy footprint consumption. Furthermore, Grand Canonical Monte Carlo simulations confirmed that the pore surface of the **NUM-11** framework enabled preferential binding of C_2H_2 over C_2H_4 and CO_2 via multiple C–H···O, C–H···π, and C–H···C interactions. This work provides some insights to prepare stable MOF materials toward the purification of C_2H_2, and the water-stable structure, low isosteric heat, and good cycling stability of **NUM-11** make it very promising for practical industrial application.

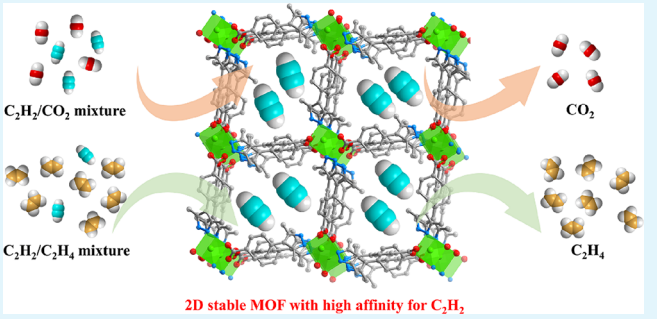

KEYWORDS: *water-stable MOF, adsorption and separation, C_2H_2 separation, GCMC simulation, structure–property relationship*

INTRODUCTION

Acetylene (C_2H_2) and ethylene (C_2H_4) are the main petrochemicals considered as basic building blocks in the petrochemical industry. C_2H_4 is widely used to manufacture kinds of chemicals, such as polyethylene and vinyl chloride.[1] C_2H_2, as the simplest alkyne, is extensively used as fuel in cutting/welding and is one of the important chemical raw materials for production of numerous synthetic chemicals such as acrylic acid and vinyl chloride.[2] In the petrochemical industry, C_2H_4 is primarily produced via steam cracking of hydrocarbons, which inevitably coexists with a trace amount of C_2H_2. The existence of C_2H_2 would poison the catalysts during ethylene polymerization.[3] Meanwhile, C_2H_2 is mainly produced by partial combustion of natural gas and/or the cracking of hydrocarbons, which are inevitably mixed with a small amount of C_2H_4 and carbon dioxide (CO_2).[4] Thus, the selective separation of C_2H_2 from CO_2 or C_2H_4 is the key to obtaining high-quality C_2H_2 and preparing polymer-grade C_2H_4. However, in light of analogous molecular structures, such as unsaturated carbon–oxide and carbon–carbon bonds, and their similar physical properties including their kinetic diameter (C_2H_2: 3.3 Å, CO_2: 3.3 Å, C_2H_4: 4.2 Å), molecular sizes (C_2H_2: 3.32 × 3.34 × 5.70 Å^3, CO_2: 3.18 × 3.33 × 5.36 Å^3, C_2H_4: 3.28 × 4.18 × 4.84 Å^3), and boiling points (C_2H_2: 189.3 K, CO_2: 194.7 K, C_2H_4: 169.4 K) (Scheme 1),[5,6] the separation of C_2H_2 from C_2H_2/C_2H_4 and C_2H_2/CO_2 mixtures is still a significant and intricate industrial separation process.[7−9] Therefore, there is an urgent need to develop effective methods to purify C_2H_2 to achieve the application requirements. Currently, the purification of C_2H_2 mainly depends on organic solvent extraction or cryogenic distillation, which is environmentally unfriendly, consumes enormous energy, and is accompanied by potential safety hazards.[10]

Received: June 3, 2022
Accepted: June 29, 2022
Published: July 12, 2022

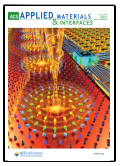

Scheme 1. Structures and Electrostatic Potentials of (a) C_2H_2, (b) CO_2, and (c) C_2H_4

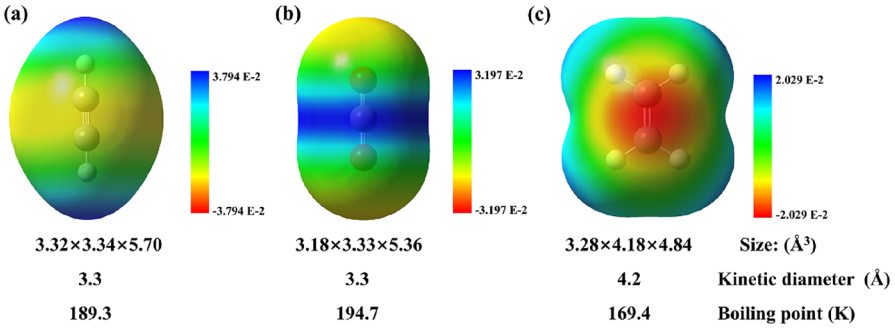

Compared with previous prevailing technologies, nonheat-driven processes such as an adsorptive separation method based on a physical adsorption mechanism could provide an alternative that has a lower energy consumption and is environmentally friendly.[11−14]

The adsorptive separation method using selective porous solid materials in light of a physical adsorption mechanism is an effective alternative strategy to energy-intensive cryogenic distillations for greener and efficient separation of C_2H_2 from C_2H_2-containing mixtures. The capability for adsorption and separation is mainly influenced by the characteristics of adsorbents, and advances in the science of solid porous materials have promoted the production of kinds of adsorbents with adjustable pore sizes and modifiable function surfaces. Under this background, the development of C_2H_2-selective multifunctional adsorbents is desperately desired to achieve the goal of related gas separation applications. Some porous solid adsorbents have been used for the C_2H_2/CO_2 or C_2H_2/C_2H_4 separation, such as zeolites (Ni@FAU)[15] and hydrogen-bonded organic frameworks (HOFs) (HOF-3, PFC-2).[16,17] Great progress has been made in the application of separation of C_2H_2/C_2H_4[3,18−22] and C_2H_2/CO_2[4,23,24] mixtures by a series of framework-type porous solid adsorbents, especially the emerging metal−organic frameworks. Metal−organic frameworks (MOFs), or porous coordination polymers (PCPs), are porous crystalline solid materials composed by metal or metal clusters as inorganic nodes and organic ligands as linkers.[25,26] MOF adsorbents show excellent prospects for adsorption and separation because the host−guest interactions could be adjusted by fine-tuning of the pore environment based on the modular nature of reticulated chemistry, and the host−guest interactions play an important role in adsorptive separation processes. In addition, in the industrial implementation, the stable MOF adsorbents are highly desired, and the stability of MOF adsorbents could be influenced by many factors, including the applied environment, organic ligands, metal ions, coordination geometry, hydrophobicity of the framework, etc. Generally, the relatively unstable coordination bonds are considered to be a major factor affecting the limited stability of MOFs. The trend of metal−ligand bond strength is in line with the hard soft acid base principle. The water stability of MOF adsorbents could be achieved by regulating the hydrophobicity of the framework, especially by embedding the hydrophobic group into the organic linkers, such as methyl groups. Nowadays, the development of stable MOF materials, especially water- or humid-stable, is highly desired in the industrial practical implementation.

Herein, we report a two-dimensional (2D) Cu-MOF, **NUM-11** ($[Cu(Hmpba)_2]\cdot 1.5DMF$), which possesses excellent stability in water, organic solvents, and a wide pH range. This MOF was constructed by a Cu(II) salt and a N,O-containing organic ligand based on the principle of hard soft acid base, and the strong hydrophobicity is mainly due to the methyl group on the organic linker. The gas separation performance of **NUM-11a** (activated **NUM-11**) shows selectivity toward C_2H_2, which could efficiently separate C_2H_2 from C_2H_2/C_2H_4, C_2H_2/CO_2, and $C_2H_2/C_2H_4/CO_2$ mixtures. The adsorption ability for C_2H_2, C_2H_4, and CO_2 was evaluated by single-component gas adsorption isotherms, and the selectivity toward C_2H_2 was proven by the heat of adsorption. The separation performances of C_2H_2 from C_2H_2/C_2H_4, C_2H_2/CO_2, and $C_2H_2/C_2H_4/CO_2$ mixtures were confirmed by IAST selectivity calculations and transient column breakthrough experiments. The mechanism of C_2H_2 purification was visually explained by Grand Canonical Monte Carlo (GCMC) simulations. Furthermore, the low adsorption heat and good cycling stability indicated its promising candidate adsorbents for the actual separation of C_2H_2 from C_2H_2/C_2H_4, C_2H_2/CO_2, and $C_2H_2/C_2H_4/CO_2$ mixtures in industrial implementation.

EXPERIMENTAL SECTION

Materials and Physical Measurements. Various chemical reagents and solvents used in this work were obtained from commercial suppliers and used directly without further purification. Powder X-ray diffraction (PXRD) data were gathered on a Rigaku Miniflex 600 at 40 kV and 15 mA using Cu-Kα radiation in an air atmosphere at a scan rate of 5.0 deg min^{-1}. Thermogravimetric analyses (TGA) were performed on a Rigaku standard TG-DTA analyzer from room temperature to 800 °C under an air atmosphere with a heating rate of 10 °C min^{-1} using an empty and clean Al_2O_3 crucible as a reference. In situ variable temperature PXRD (VT-PXRD) patterns were collected on a Bruker D8 diffractometer. The surface morphology of the samples was analyzed by scanning electron microscopy (SEM) (JOEL JSM-7800F).

Synthesis of NUM-11. A mixture of $Cu(NO_3)_2\cdot 3H_2O$ (0.15 g), 4-(3,5-dimethyl-1*H*-pyrazol-4-yl)benzoic acid (H_2mpba) (0.05 g), *N*,*N*-dimethylformamide (DMF) (10 mL), and H_2O (10 mL) was placed in a 50 mL screw-capped glass vial, and the suspension became homogeneous by sonicating; then, the glass vial was capped and heated in an oven at 353 K for 12 h. After it was cooled naturally to room temperature, violet rectangular block crystals were obtained and washed several times with DMF to afford **NUM-11** (yield: about 72% based on H_2mpba) (CCDC number: 2142649). The desolvated sample used for gas adsorption measurement was prepared by a methanol-exchanged sample followed by activation under ultrahigh vacuum conditions at 150 °C for 8 h.

Single-Component Gas Adsorption Measurements. N_2 sorption measurements were performed at 77 K with a liquid nitrogen bath using a Micrometrics ASAP 2460 volumetric gas adsorption analyzer in a pressure range from 0 to 1.1 bar. The

https://doi.org/10.1021/acsami.2c09917
ACS Appl. Mater. Interfaces 2022, 14, 33429−33437

sorption isotherms of C_2H_2, C_2H_4, and CO_2 were measured at different temperatures (278, 288, and 298 K) controlled with a circulating water bath (Julabo F12) through a fully automatic gas adsorption analyzer (Micromeritics, ASAP 2020 HD88). The gases used for sorption measurements were provided with ultrahigh purities.

GCMC Simulations. The GCMC simulations were carried out for the adsorption of C_2H_2, C_2H_4, and CO_2 in **NUM-11a** using the sorption module in Materials Studio. The skeleton of **NUM-11a** and gas molecules were regarded as rigid bodies. The optimal adsorption sites were simulated under 298 K and 1.0 bar by the fixed loading task and Metropolis method. The loading steps, equilibration steps, and production steps were all set to 5.0×10^6. The gas−skeleton interaction and the gas−gas interaction were characterized by the standard universal force field (UFF). The atomic partial charges of the host skeleton of **NUM-11a** were obtained from DDEC calculations.[27,28] The cutoff radius used for the Lennard-Jones interactions was 15.5 Å.

RESULTS AND DISCUSSION

The reaction of H_2mpba and $Cu(NO_3)_2{\cdot}3H_2O$ under solvothermal conditions produced a porous framework **NUM-11** (Figure 1). In the MOF, Cu^{2+} in the metal center

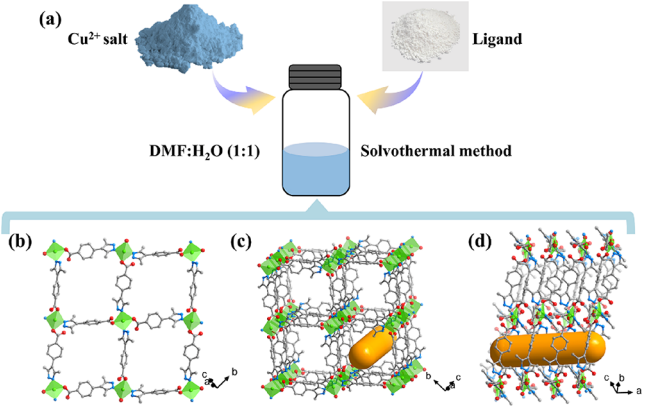

Figure 1. (a) Scheme for the synthesis of **NUM-11**. Microstructure of **NUM-11**: (b) two-dimensional framework, (c) one-dimensional channel, and (d) 2D layers stacked together through $\pi-\pi$ interactions. C, gray; O, red; Cu, green; and N, blue. Hydrogen atoms and solvent molecules were omitted for clarity.

adopts a planar four-coordination mode, which is coordinated with pyrazole groups (with two N atoms) and two carboxylate groups (with two O atoms) (Figure S1), generating a two-dimensional square lattice (*sql*) coordination framework (Figure 1b,c and Figure S2). The layered network structure is further stacked together through $\pi-\pi$ interactions (Figure 1d and Figure S3). The MOF material has been fully characterized by PXRD, scanning electron microscopy, in situ VT-PXRD, and thermogravimetric analysis. The synthesized bulk sample phase purity was confirmed by comparing the experimental PXRD pattern with the simulated one exported from the single crystal structure data (Figure S4). The filled guest solvents in the pore channels can be completely removed through vacuum heating at 150 °C for 8 h, getting the desolvated sample. This desolvated sample has the same structure as **NUM-11**.[29] After the free DMF guest molecules in the channel were removed from the as-synthesized sample, the desolvated material shows a similar PXRD pattern to the as-synthesized one, which verifies the stability upon guest loss (Figure S5). In addition, the desolvated MOF exhibits a one-dimensional (1D) channel with a pore size of approximately 5.7×6.3 Å^2 along the *a*-axis.

The scanning electron microscopy image presented in Figure 2a distinctly exhibits the rectangular block morphology of **NUM-11** crystals. From the optical microscopy image (Figure 2b), it is confirmed that this MOF with violet cubic shape was well-crystallized. According to the hard soft acid base principle, **NUM-11** was constructed by the Cu^{2+} node and N,O-containing organic linker, which may show modest thermal stability. Then, the thermal stability of **NUM-11** was first proven by TGA and VT-PXRD (Figure 2c,d). The thermogravimetric curve and VT-PXRD patterns exhibit that **NUM-11** can maintain the framework structure up to approximately 320 °C, and the results of VT-PXRD were consistent well with the TG curve. Since the methyl group is embedded on the ligand, then water stability is elaboratively studied. As shown in Figure 2e,f, **NUM-11** shows good stability in aqueous solution with a wide pH range and different temperatures. Due to the synergistic effect of the hard soft acid base principle and methyl functional group, **NUM-11** is an excellent water-stable candidate MOF adsorbent. The excellent chemical and thermal stabilities and especially water stability, which is extremely desired, make this MOF material practically available.

Prior to single-component gas adsorption experiments, **NUM-11** was activated by heating the methanol-exchanged sample to 423 K for 8 h under a high vacuum atmosphere ($<10^{-5}$ torr) to obtain the desolvated sample **NUM-11a**. The PXRD pattern of the desolvated sample indicated that the framework architecture of this MOF can be maintained. The permanent porosity of **NUM-11a** was assessed by N_2 adsorption at 77 K and CO_2 adsorption at 195 K. The single-component gas adsorption capacities of N_2 and CO_2 for **NUM-11a**·are 11.24 and 88.70 cm^3 g^{-1}, respectively (Figure 3a). The Brunauer−Emmett−Teller (BET) surface area of **NUM-11a**·was determined to be 374.2 m^2 g^{-1} based on the CO_2 adsorption isotherm at 195 K. Apparently, no considerable uptake amount is observed in the N_2 sorption isotherms at 77 K, probably owing to the strong host−guest interactions between the N_2 guest molecule and the channel windows, blocking N_2 diffusion into the MOF, and the low kinetic energy of N_2.[30−32]

Motivated by the stable structure, the gas adsorption and separation behavior of **NUM-11a**·was explored. First, the low pressure pure-component gas adsorption isotherms for C_2H_2, C_2H_4, and CO_2 at different temperatures (278, 288, and 298 K) were measured. As shown in Figure 3b−d, the adsorption capacity of C_2H_2 on **NUM-11a** is obviously higher than those of C_2H_4 and CO_2. Specifically, the uptake amounts of C_2H_2, C_2H_4, and CO_2 for **NUM-11a** are 50.51, 35.85, and 28.42 cm^3 g^{-1} at 298 K and 1.0 bar, which represents that C_2H_2 is more preferentially adsorbed than C_2H_4 and CO_2 in the ultramicroporous channels. In short, the adsorption capacity of C_2H_2 (2.25 mmol g^{-1}) is modest for **NUM-11a** at 298 K and 1.0 bar, higher than or comparable to many well-known MOFs, such as Cu-FINA-2 (approximately 1.79 mmol g^{-1}),[33] CPL-1 (1.84 mmol g^{-1}) and CPL-1-NH$_2$ (2.01 mmol g^{-1}),[34] M'MOF-3a (1.90 mmol g^{-1}),[35] UiO-66-(COOH)$_2$ (2.16 mmol g^{-1}),[36] JNU-1 (2.67 mmol g^{-1}),[37] Ni$_3$(pzdc)$_2$(7Hade)$_2$ (2.36 mmol g^{-1}),[38] NKMOF-1-Cu (2.27 mmol g^{-1}),[8] and Cu^I@UiO-66-(COOH)$_2$ (2.31 mmol g^{-1}).[36] **NUM-11a** shows relatively small CO_2 adsorption amounts (1.27 mmol g^{-1}) under the same situations, resulting in a well C_2H_2/CO_2

https://doi.org/10.1021/acsami.2c09917
ACS Appl. Mater. Interfaces 2022, 14, 33429−33437

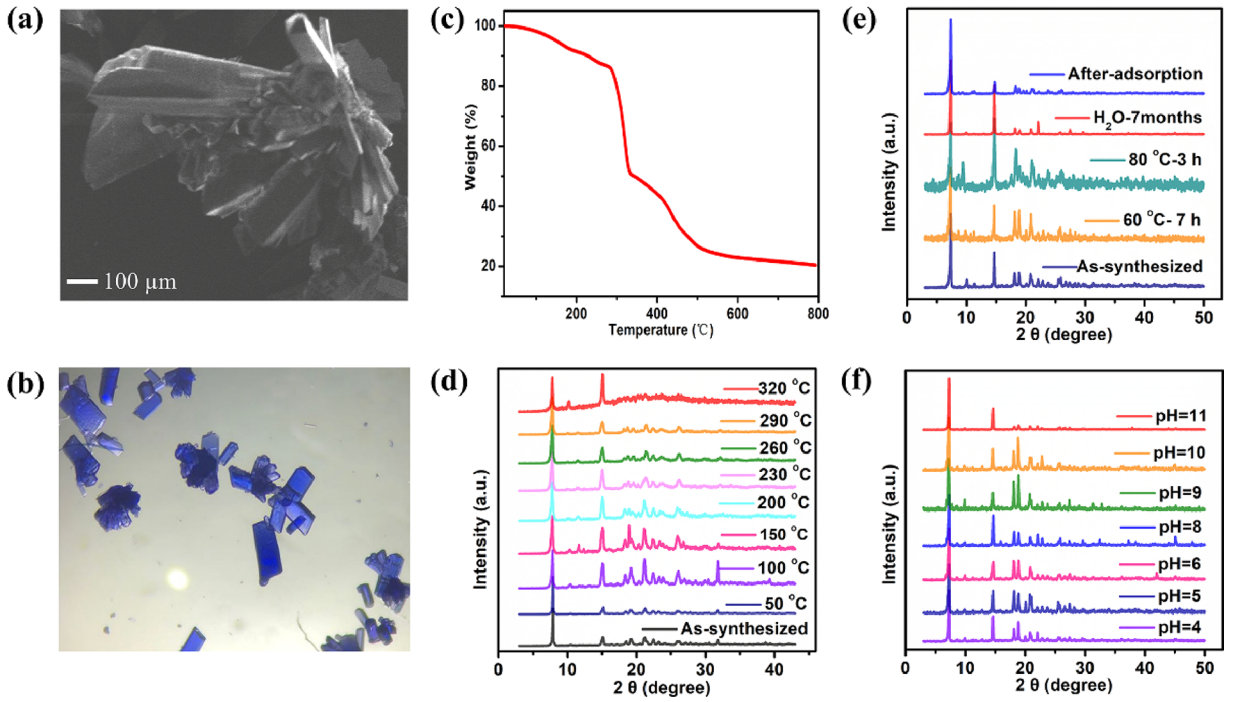

Figure 2. (a) SEM image and (b) optical microscope image of the crystal of **NUM-11**. (c) TG curve of **NUM-11**. (d) VT-PXRD patterns of **NUM-11** under an air atmosphere. (e) PXRD patterns of **NUM-11** soaked in water with different temperatures and times. (f) PXRD patterns of **NUM-11** soaked in different pH aqueous solvents for 24 h.

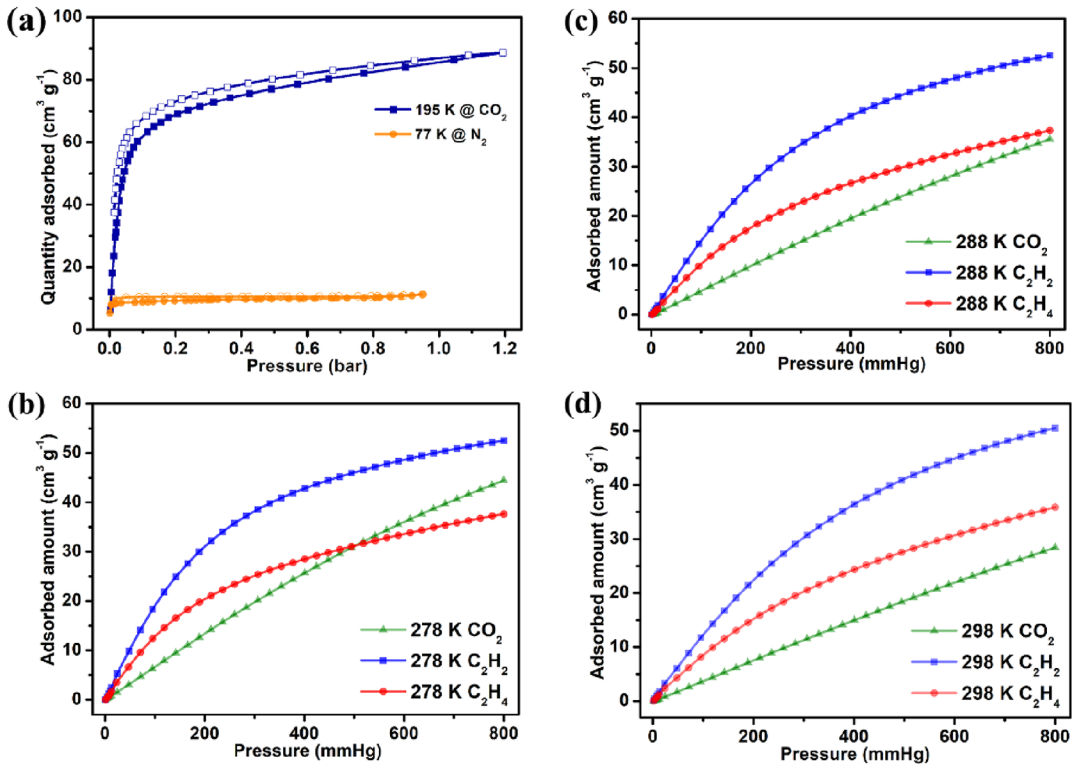

Figure 3. Adsorption data of **NUM-11a**. (a) N_2 (orange) sorption isotherms at 77 K and CO_2 (violet) at 195 K. Single-component gas adsorption isotherms for C_2H_2 (blue), C_2H_4 (red), and CO_2 (green) (b) at 278 K, (c) at 288 K, and (d) at 298 K.

uptake ration of 1.78, higher than or comparable to those of UiO-66-$(COOH)_2$ (1.29),[36] JNU-2 (2.1),[39] etc. In addition, the small adsorption amount for C_2H_4 also causes a modest C_2H_2/C_2H_4 uptake ratio of 1.3, comparable to that of NKMOF-1-Ni (1.28),[8] FeMOF-74 (1.11),[40] and NOTT-300 (1.48).[41] The single-component gas adsorption performance shows that the strong C_2H_2 binding affinity in **NUM-11a** is promising to be used for separation of C_2H_2 from mixtures containing CO_2 and C_2H_4. Based on this kind of gas adsorption behavior, we focused on the separation potential

https://doi.org/10.1021/acsami.2c09917
ACS Appl. Mater. Interfaces 2022, 14, 33429−33437

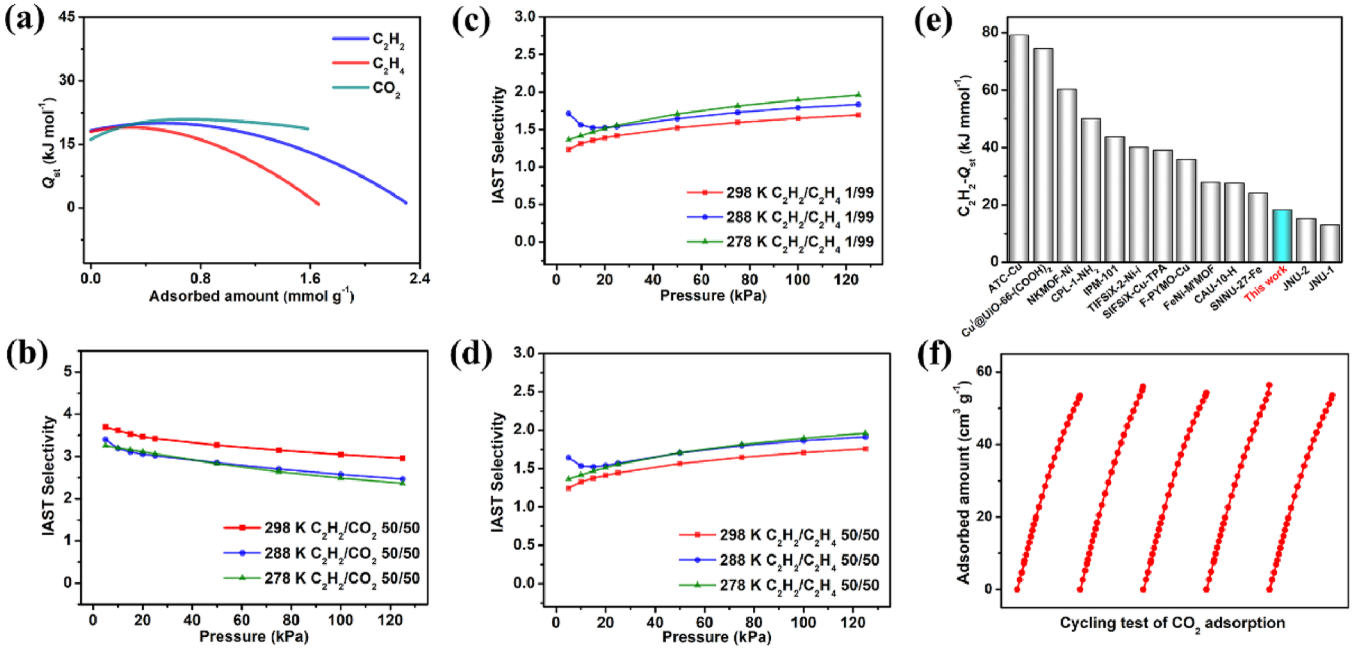

Figure 4. (a) Adsorption enthalpy of C_2H_2, C_2H_4, and CO_2 on **NUM-11a**, calculated from the single-component adsorption data at 278 and 288 K. Predicted adsorption selectivity of **NUM-11a** by using the IAST method for the (b) 50/50 (v/v) C_2H_2/CO_2 mixture, (c) 1/99 (v/v) C_2H_2/C_2H_4 mixture, and (d) 50/50 (v/v) C_2H_2/C_2H_4 mixture. (e) Comparison of the C_2H_2-Q_{st} of **NUM-11a** at low coverage and other best-performing materials for separation of C_2H_2/CO_2. (f) Cycling test of CO_2 adsorption measurements at 273 K.

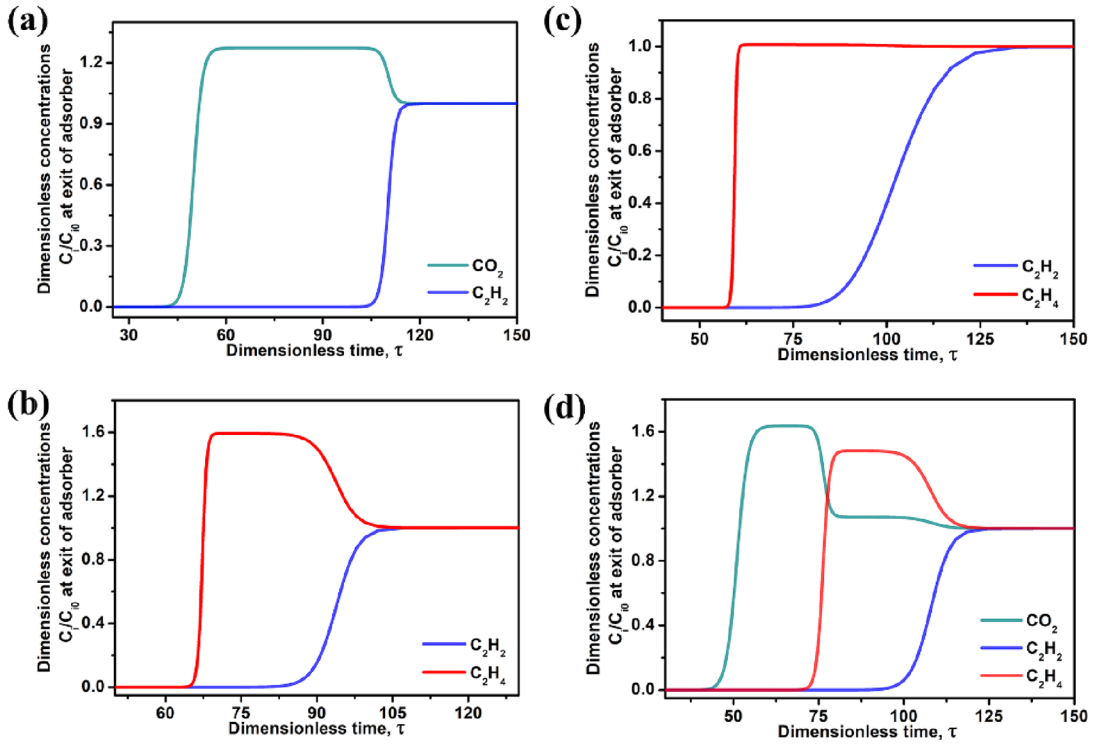

Figure 5. Transient breakthrough simulations of C_2H_2/C_2H_4, C_2H_2/CO_2, and $C_2H_2/C_2H_4/CO_2$ mixtures in an adsorber bed packed using **NUM-11a** at 298 K. Different operating conditions were (a) C_2H_2/CO_2 (50/50, v/v), (b) C_2H_2/C_2H_4 (50/50, v/v), (c) C_2H_2/C_2H_4 (1/99, v/v), and (d) equimolar $C_2H_2/C_2H_4/CO_2$ mixtures.

of C_2H_2/CO_2, C_2H_2/C_2H_4, and $C_2H_2/C_2H_4/CO_2$ mixtures because of their practical application relevance.

In order to evaluate the host−guest interactions between the framework and guest molecules, the coverage-dependent isosteric adsorption heats (Q_{st}) of **NUM-11a** for C_2H_2, C_2H_4, and CO_2 were calculated by a virial equation method using the single-component adsorption data collected at 278 and 288 K. As shown in Figure 4a, the Q_{st} value of C_2H_2 on **NUM-11a** at zero-loading was 18.24 kJ mol^{-1}, whereas the Q_{st} values for C_2H_4 and CO_2 were 17.99 and 16.14 kJ mol^{-1}, respectively. The higher Q_{st} value indicates a strong binding affinity toward C_2H_2 over C_2H_4 and CO_2 on **NUM-11a**. In

https://doi.org/10.1021/acsami.2c09917
ACS Appl. Mater. Interfaces 2022, 14, 33429−33437

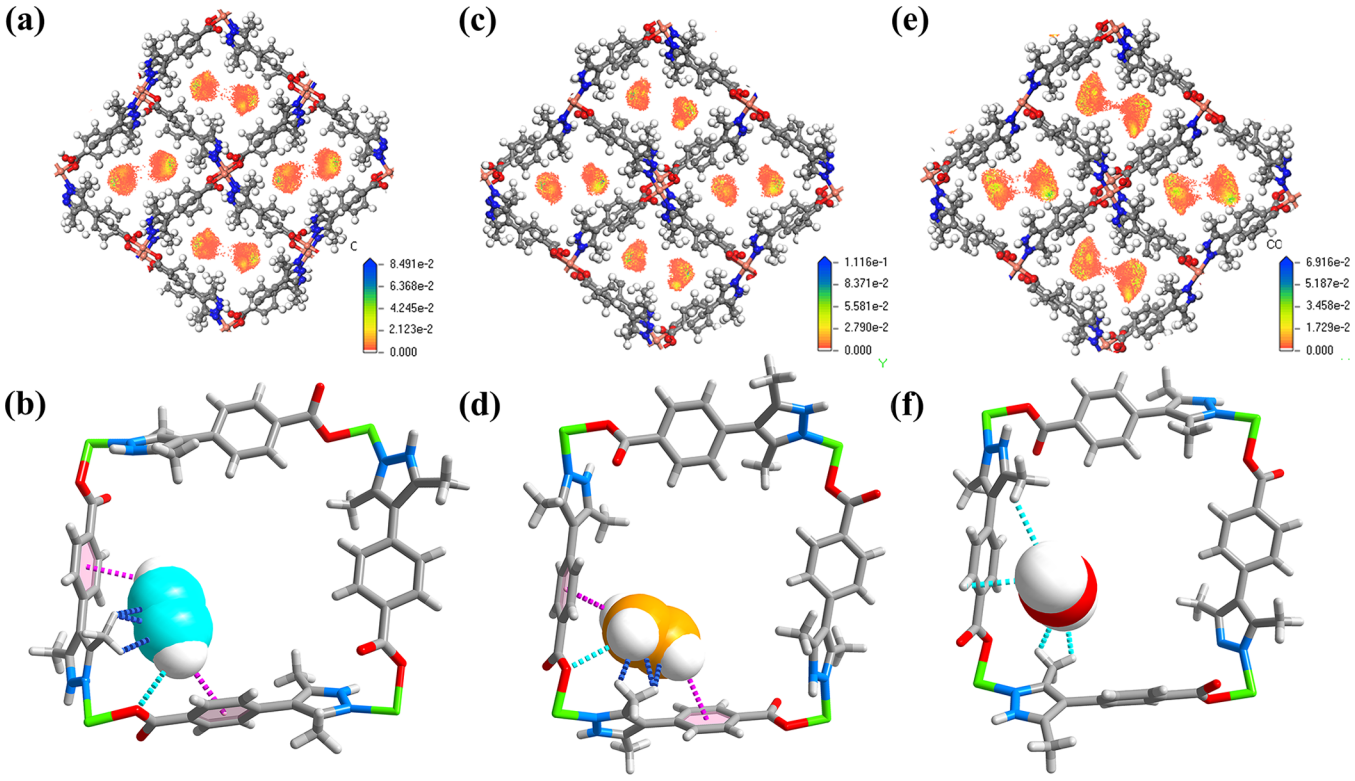

Figure 6. Adsorption density distribution and possible binding sites calculated by GCMC simulation at 298 K and 1.0 bar for (a, b) C_2H_2, (c, d) C_2H_4, and (e, f) CO_2 in **NUM-11a**. C, gray; O, red; Cu, green; and H, white.

addition, the result of Q_{st} agrees well with the tendency of adsorption performance, which proves once again the feasibility for the separation of C_2H_2 from the C_2H_2/CO_2, C_2H_2/C_2H_4, and $C_2H_2/C_2H_4/CO_2$ mixtures. Notably, the Q_{st} value for C_2H_2 is lower than those of previously reported MOFs such as CPL-1-NH_2 (50 kJ $mmol^{-1}$),[34] NKMOF-1-Ni (60.3 kJ $mmol^{-1}$),[8] TIFSIX-2-Ni-i (40 kJ $mmol^{-1}$),[42] F-PYMO-Cu (35.9 kJ $mmol^{-1}$), Cu^I@UiO-66-$(COOH)_2$ (74.5 kJ $mmol^{-1}$),[36] FeNi-M'MOF (27−32.8 kJ $mmol^{-1}$),[40] SIFSIX-Cu-TPA (39.1 kJ $mmol^{-1}$),[43] sql-SIFSIX-bpe-Zn (67.5 kJ $mmol^{-1}$),[44] and UTSA-74a (31 kJ $mmol^{-1}$)[45] (Figure 4e). Such a low adsorption enthalpy for C_2H_2 not only implies the feasibility to easily regenerate the MOF material under mild conditions but also suggests the lower energy footprints consumed in the regeneration of the MOF.

Inspired by the distinct adsorption interaction differences in C_2H_2, CO_2, and C_2H_4 toward the 2D stable MOF material, **NUM-11a** has promising potential for efficient separation of C_2H_2 from C_2H_2/C_2H_4 and C_2H_2/CO_2 mixtures. The separation capacity toward C_2H_2/C_2H_4 and C_2H_2/CO_2 was evaluated in light of the ideal adsorbed solution theory (IAST) method. The detailed calculation of adsorption selectivity using the IAST theory is shown in the Supporting Information. As shown in Figure 4b−d, the calculated selectivity values of C_2H_2/C_2H_4 (1/99, v/v) and C_2H_2/CO_2 (50/50, v/v) mixtures, whose composition is close to actual industrial mixtures, are 1.65 and 3.00, respectively. Compared with some reported MOFs, the selectivity value of C_2H_2/CO_2 (50/50) is higher than that of some MOFs including UPC-200(M)-R-L series (1.89−2.25),[23] SNNU-27-M (1.0−2.0),[46] etc. In addition, the C_2H_2/C_2H_4 (1/99) selectivity value is higher than or comparable to those of NPU-1 (1.4) and NPU-2 (1.25).[47] These endow the C_2H_2 purification with proficiency for **NUM-11a**. Continuous CO_2 adsorption/desorption experiments on **NUM-11a**·were carried out to evaluate its cycling stability. After five cycles, **NUM-11a**·shows no obvious reduction in its CO_2 adsorption capacities (Figure 4f).

In order to appraise the practicable separation of C_2H_2 from the mixtures containing C_2H_4 and CO_2 for **NUM-11a**, transient breakthrough simulations were conducted for the separation of C_2H_2/C_2H_4 (10/90 and 50/50, v/v), C_2H_2/CO_2 (50/50, v/v), and equimolar $C_2H_2/C_2H_4/CO_2$ mixtures in a fixed-bed utilizing a pressure swing adsorption operation at 298 K. As shown in Figure 5, a function of the dimensionless time, τ, in the transient breakthrough can be used to illustrate the separation performance. Due to the stronger interactions between C_2H_2 molecules and the framework than those of C_2H_4 and CO_2, C_2H_4 and CO_2 first eluted out from the column at the beginning of the experiment, while C_2H_2 was still adsorbed. This series of breakthrough curves confirm that **NUM-11a** could be a good candidate for the separation of C_2H_2 from C_2H_4 and CO_2.

The differences in gas adsorption capacity and isosteric adsorption heat among C_2H_2, CO_2, and C_2H_4 suggest the potential of **NUM-11a** for the separation of C_2H_2 from C_2H_2/CO_2, C_2H_2/C_2H_4, and $C_2H_2/C_2H_4/CO_2$ mixtures. In order to gain profound insights into the adsorption behavior and visually understand the host−guest interactions between the framework and the guest molecules, we performed detailed theoretical investigations using GCMC simulations to investigate the adsorption density distribution and possible binding sites of C_2H_2, CO_2, and C_2H_4. As shown in Figure 6, in light of the adsorption density distribution, the favorable adsorption sites of C_2H_2, C_2H_4, and CO_2 were distributed at the corner near the aromatic rings and the methyl groups. The results of the possible binding sites reveal that the probable

https://doi.org/10.1021/acsami.2c09917
ACS Appl. Mater. Interfaces 2022, 14, 33429−33437

binding site for C_2H_2 is located between two adjacent benzene rings and C_2H_2 interacts with the framework through forming three C−H···C (3.118−3.334 Å), one C−H···O (3.356 Å), and two C−H···π (3.232−3.306 Å) interactions (Figure 6a,b). Similar to C_2H_2, C_2H_4 also interacts with the framework through forming three C−H···C (3.348−3.432 Å), one C−H···O (3.359 Å), and two C−H···π (3.260−3.266 Å) interactions, while the distance is longer (Figure 6c,d). CO_2 interacts with the framework through forming four C−H···O (3.105−3.616 Å) interactions (Figure 6e,f). As a result, C_2H_2 interacts much stronger with the framework than CO_2 and C_2H_4, mainly because of the superposition of multiple weak interactions. Therefore, it could be inferred from the above discussion that the strong interaction drives the high C_2H_2 binding affinity and decent purification capacity of C_2H_2. These theoretical calculation results are consistent well with the experimental phenomena.

CONCLUSIONS

In summary, we have investigated the use of a N,O-containing organic linker to construct a two-dimensional MOF **NUM-11**, with ultrahigh water stability, featuring a simple *sql* topology and rhombic pores, for the separation of C_2H_2 from C_2H_4 and CO_2. With the advantages of stable framework, decent single-component gas adsorption behavior and C_2H_2/CO_2, C_2H_2/C_2H_4, and $C_2H_2/C_2H_4/CO_2$ separation performance, low adsorption enthalpy, good regeneration properties, and outstanding recycle ability, **NUM-11a** is considered to be a promising candidate for critical industrial applications. In addition, the mechanism over the selectivity adsorption/separation from the molecular level is visually revealed by GCMC simulations. This work not only reports a stable MOF for the C_2H_2/CO_2, C_2H_2/C_2H_4, and $C_2H_2/C_2H_4/CO_2$ separation but also provides guidance for the synthesis of stable MOFs, making use of the synergistic effect of the hard soft acid base principle and protective groups.

ASSOCIATED CONTENT

Supporting Information

The Supporting Information is available free of charge at https://pubs.acs.org/doi/10.1021/acsami.2c09917.

Full experimental details, including crystal structure, PXRD patterns, C_2H_2, C_2H_4, and CO_2 sorption data, and breakthrough simulations (PDF)

Crystallographic data of **NUM-11** (CIF)

AUTHOR INFORMATION

Corresponding Author

Tong-Liang Hu − *School of Materials Science and Engineering, National Institute for Advanced Materials, Nankai University, Tianjin 300350, China;* orcid.org/0000-0001-9619-9867; Email: tlhu@nankai.edu.cn

Authors

Shan-Qing Yang − *School of Materials Science and Engineering, National Institute for Advanced Materials, Nankai University, Tianjin 300350, China*

Lei Zhou − *School of Materials Science and Engineering, National Institute for Advanced Materials, Nankai University, Tianjin 300350, China*

Yabing He − *Key Laboratory of the Ministry of Education for Advanced Catalysis Materials, College of Chemistry and Life Sciences, Zhejiang Normal University, Jinhua 321004, China;* orcid.org/0000-0002-0094-0591

Rajamani Krishna − *Van't Hoff Institute for Molecular Sciences, University of Amsterdam, Amsterdam 1098 XH, The Netherlands;* orcid.org/0000-0002-4784-8530

Qiang Zhang − *School of Materials Science and Engineering, National Institute for Advanced Materials, Nankai University, Tianjin 300350, China*

Yi-Feng An − *School of Materials Science and Engineering, National Institute for Advanced Materials, Nankai University, Tianjin 300350, China*

Bo Xing − *School of Materials Science and Engineering, National Institute for Advanced Materials, Nankai University, Tianjin 300350, China*

Ying-Hui Zhang − *School of Materials Science and Engineering, National Institute for Advanced Materials, Nankai University, Tianjin 300350, China*

Complete contact information is available at: https://pubs.acs.org/10.1021/acsami.2c09917

Notes

The authors declare no competing financial interest.

ACKNOWLEDGMENTS

This work was financially supported by the Natural Science Foundation of Tianjin (20JCYBJC01330) and the National Natural Science Foundation of China (21673120).

REFERENCES

(1) Sholl, D. S.; Lively, R. P. Seven Chemical Separations to Change the World. *Nature* **2016**, *532*, 435−437.

(2) Schobert, H. Production of Acetylene and Acetylene-based Chemicals from Coal. *Chem. Rev.* **2014**, *114*, 1743−1760.

(3) Hu, T.-L.; Wang, H.; Li, B.; Krishna, R.; Wu, H.; Zhou, W.; Zhao, Y.; Han, Y.; Wang, X.; Zhu, W.; Yao, Z.; Xiang, S.; Chen, B. Microporous Metal-Organic Framework with Dual Functionalities for Highly Efficient Removal of Acetylene from Ethylene/Acetylene Mixtures. *Nat. Commun.* **2015**, *6*, 7328.

(4) Matsuda, R.; Kitaura, R.; Kitagawa, S.; Kubota, Y.; Belosludov, R. V.; Kobayashi, T. C.; Sakamoto, H.; Chiba, T.; Takata, M.; Kawazoe, Y.; Mita, Y. Highly Controlled Acetylene Accommodation in a Metal-Organic Microporous Material. *Nature* **2005**, *436*, 238−241.

(5) Li, J.-R.; Kuppler, R. J.; Zhou, H.-C. Selective Gas Adsorption and Separation in Metal-Organic Frameworks. *Chem. Soc. Rev.* **2009**, *38*, 1477−1504.

(6) Reid, C. R.; Thomas, K. M. Adsorption Kinetics and Size Exclusion Properties of Probe Molecules for the Selective Porosity in a Carbon Molecular Sieve used for Air Separation. *J. Phys. Chem. B* **2001**, *105*, 10619−10629.

(7) Chen, K.-J.; Scott, H. S.; Madden, D. G.; Pham, T.; Kumar, A.; Bajpai, A.; Lusi, M.; Forrest, K. A.; Space, B.; Perry, J. J., IV; Zaworotko, M. J. Benchmark C_2H_2/CO_2 and CO_2/C_2H_2 Separation by Two Closely Related Hybrid Ultramicroporous Materials. *Chem* **2016**, *1*, 753−765.

(8) Peng, Y.-L.; Pham, T.; Li, P.; Wang, T.; Chen, Y.; Chen, K.-J.; Forrest, K. A.; Space, B.; Cheng, P.; Zaworotko, M. J.; Zhang, Z. Robust Ultramicroporous Metal-Organic Frameworks with Benchmark Affinity for Acetylene. *Angew. Chem., Int. Ed.* **2018**, *57*, 10971−10975.

(9) Peh, S. B.; Farooq, S.; Zhao, D. A Metal-Organic Framework (MOF)-based Temperature Swing Adsorption Cycle for Postcombustion CO_2 Capture from Wet Flue Gas. *Chem. Eng. Sci.* **2022**, No. 117399.

(10) Chen, K.-J.; Madden, D. G.; Mukherjee, S.; Pham, T.; Forrest, K. A.; Kumar, A.; Space, B.; Kong, J.; Zhang, Q.-Y.; Zaworotko, M. J.

Synergistic Sorbent Separation for One-Step Ethylene Purification from a Four-Component Mixture. *Science* **2019**, *366*, 241−246.
(11) Cui, W.-G.; Hu, T.-L.; Bu, X.-H. Metal-Organic Framework Materials for the Separation and Purification of Light Hydrocarbons. *Adv. Mater.* **2020**, *32*, 1806445.
(12) Yang, S.-Q.; Sun, F.-Z.; Krishna, R.; Zhang, Q.; Zhou, L.; Zhang, Y.-H.; Hu, T.-L. Propane-Trapping Ultramicroporous Metal-Organic Framework in the Low-Pressure Area toward the Purification of Propylene. *ACS Appl. Mater. Interfaces* **2021**, *13*, 35990−35996.
(13) Sun, F.-Z.; Yang, S.-Q.; Krishna, R.; Zhang, Y.-H.; Xia, Y.-P.; Hu, T.-L. Microporous Metal-Organic Framework with a Completely Reversed Adsorption Relationship for C_2 Hydrocarbons at Room Temperature. *ACS Appl. Mater. Interfaces* **2020**, *12*, 6105−6111.
(14) Yu, M.-H.; Space, B.; Franz, D.; Zhou, W.; He, C.; Li, L.; Krishna, R.; Chang, Z.; Li, W.; Hu, T.-L.; Bu, X.-H. Enhanced Gas Uptake in a Microporous Metal-Organic Framework via a Sorbate Induced-Fit Mechanism. *J. Am. Chem. Soc.* **2019**, *141*, 17703−17712.
(15) Chai, Y.; Han, X.; Li, W.; Liu, S.; Yao, S.; Wang, C.; Shi, W.; da Silva, I.; Manuel, P.; Cheng, Y.; Daemen, L. D.; Ramirez-Cuesta, A. J.; Tang, C. C.; Jiang, L.; Yang, S.; Guan, N.; Li, L. Control of Zeolite Pore Interior for Chemoselective Alkyne/Olefin Separations. *Science* **2020**, *368*, 1002−1006.
(16) Li, P.; He, Y.; Zhao, Y.; Weng, L.; Wang, H.; Krishna, R.; Wu, H.; Zhou, W.; O'Keeffe, M.; Han, Y.; Chen, B. A Rod-Packing Microporous Hydrogen-Bonded Organic Framework for Highly Selective Separation of C_2H_2/CO_2 at Room Temperature. *Angew. Chem., Int. Ed.* **2015**, *54*, 574−577.
(17) Yin, Q.; Li, Y.-L.; Li, L.; Lü, J.; Liu, T.-F.; Cao, R. Novel Hierarchical Meso-Microporous Hydrogen-Bonded Organic Framework for Selective Separation of Acetylene and Ethylene versus Methane. *ACS Appl. Mater. Interfaces* **2019**, *11*, 17823−17827.
(18) Yang, S.-Q.; Sun, F.-Z.; Liu, P.; Li, L.; Krishna, R.; Zhang, Y.-H.; Li, Q.; Zhou, L.; Hu, T.-L. Efficient Purification of Ethylene from C_2 Hydrocarbons with an C_2H_6/C_2H_2-Selective Metal-Organic Framework. *ACS Appl. Mater. Interfaces* **2021**, *13*, 962−969.
(19) Cui, X.; Chen, K.; Xing, H.; Yang, Q.; Krishna, R.; Bao, Z.; Wu, H.; Zhou, W.; Dong, X.; Han, Y.; Li, B.; Ren, Q.; Zaworotko, M. J.; Chen, B. Pore Chemistry and Size Control in Hybrid Porous Materials for Acetylene Capture from Ethylene. *Science* **2016**, *353*, 141−144.
(20) Shen, J.; He, X.; Ke, T.; Krishna, R.; van Baten, J. M.; Chen, R.; Bao, Z.; Xing, H.; Dincă, M.; Zhang, Z.; Yang, Q.; Ren, Q. Simultaneous Interlayer and Intralayer Space Control in Two-Dimensional Metal-Organic Frameworks for Acetylene/Ethylene Separation. *Nat. Commun.* **2020**, *11*, 6529.
(21) Belmabkhout, Y.; Zhang, Z.; Adil, K.; Bhatt, P. M.; Cadiau, A.; Solovyeva, V.; Xing, H.; Eddaoudi, M. Hydrocarbon Recovery Using Ultra-Microporous Fluorinated MOF Platform with and without Uncoordinated Metal Sites: I-Structure Properties Relationships for C_2H_2/C_2H_4 and CO_2/C_2H_2 Separation. *Chem. Eng. J.* **2019**, *359*, 32−36.
(22) Zhang, Q.; Yang, S.-Q.; Zhou, L.; Yu, L.; Li, Z.-F.; Zhai, Y.-j.; Hu, T.-L. Pore-Space Partition through an Embedding Metal-Carboxylate Chain-Induced Topology Upgrade Strategy for the Separation of Acetylene/Ethylene. *Inorg. Chem.* **2021**, *60*, 19328−19335.
(23) Fan, W.; Yuan, S.; Wang, W.; Feng, L.; Liu, X.; Zhang, X.; Wang, X.; Kang, Z.; Dai, F.; Yuan, D.; Sun, D.; Zhou, H.-C. Optimizing Multivariate Metal-Organic Frameworks for Efficient C_2H_2/CO_2 Separation. *J. Am. Chem. Soc.* **2020**, *142*, 8728−8737.
(24) Wang, J.; Zhang, Y.; Su, Y.; Liu, X.; Zhang, P.; Lin, R.-B.; Chen, S.; Deng, Q.; Zeng, Z.; Deng, S.; Chen, B. Fine Pore Engineering in a Series of Isoreticular Metal-Organic Frameworks for Efficient C_2H_2/CO_2 Separation. *Nat. Commun.* **2022**, *13*, 200.
(25) Li, H.; Eddaoudi, M.; O'Keeffe, M.; Yaghi, O. M. Design and Synthesis of an Exceptionally Stable and Highly Porous Metal-Organic Framework. *Nature* **1999**, *402*, 276−279.
(26) Kitagawa, S.; Kitaura, R.; Noro, S.-i. Functional Porous Coordination Polymers. *Angew. Chem., Int. Ed.* **2004**, *43*, 2334−2375.
(27) Manz, T. A.; Limas, N. G. Introducing DDEC6 Atomic Population Analysis: Part 1. Charge Partitioning Theory and Methodology. *RSC Adv.* **2016**, *6*, 47771−47801.
(28) Limas, N. G.; Manz, T. A. Introducing DDEC6 Atomic Population Analysis: Part 2. Computed Results for a Wide Range of Periodic and Nonperiodic Materials. *RSC Adv.* **2016**, *6*, 45727−45747.
(29) Menzel, S.; Millan, S.; Höfert, S.-P.; Nuhnen, A.; Gökpinar, S.; Schmitz, A.; Janiak, C. Increase of Network Hydrophilicity from sql to lvt Supramolecular Isomers of Cu-MOFs with the Bifunctional 4-(3,5-dimethyl-1H-pyrazol-4-yl) Benzoate Linker. *Dalton Trans.* **2020**, *49*, 12854−12864.
(30) Shi, W.-J.; Li, Y.-Z.; Chen, J.; Su, R.-H.; Hou, L.; Wang, Y.-Y.; Zhu, Z. A New Metal-Organic Framework based on Rare $[Zn_4F_4]$ Cores for Efficient Separation of C_2H_2. *Chem. Commun.* **2021**, *57*, 12788−12791.
(31) Nugent, P. S.; Rhodus, V. L.; Pham, T.; Forrest, K.; Wojtas, L.; Space, B.; Zaworotko, M. J. A Robust Molecular Porous Material with High CO_2 Uptake and Selectivity. *J. Am. Chem. Soc.* **2013**, *135*, 10950−10953.
(32) Hazra, A.; Bonakala, S.; Adalikwu, S. A.; Balasubramanian, S.; Maji, T. K. Fluorocarbon-Functionalized Superhydrophobic Metal-Organic Framework: Enhanced CO_2 Uptake via Photoinduced Postsynthetic Modification. *Inorg. Chem.* **2021**, *60*, 3823−3833.
(33) Wu, X.-Q.; Liu, J.-H.; He, T.; Zhang, P.-D.; Yu, J.; Li, J.-R. Understanding How Pore Surface Fluorination Influences Light Hydrocarbon Separation in Metal-Organic Frameworks. *Chem. Eng. J.* **2021**, *407*, No. 127183.
(34) Yang, L.; Yan, L.; Wang, Y.; Liu, Z.; He, J.; Fu, Q.; Liu, D.; Gu, X.; Dai, P.; Li, L.; Zhao, X. Adsorption Site Selective Occupation Strategy within a Metal-Organic Framework for Highly Efficient Sieving Acetylene from Carbon Dioxide. *Angew. Chem., Int. Ed.* **2021**, *60*, 4570−4574.
(35) Xiang, S.-C.; Zhang, Z.; Zhao, C.-G.; Hong, K.; Zhao, X.; Ding, D.-R.; Xie, M.-H.; Wu, C.-D.; Das, M. C.; Gill, R.; Thomas, K. M.; Chen, B. Rationally Tuned Micropores Within Enantiopure Metal-Organic Frameworks for Highly Selective Separation of Acetylene and Ethylene. *Nat. Commun.* **2011**, *2*, 204.
(36) Zhang, L.; Jiang, K.; Yang, L.; Li, L.; Hu, E.; Yang, L.; Shao, K.; Xing, H.; Cui, Y.; Yang, Y.; Li, B.; Chen, B.; Qian, G. Benchmark C_2H_2/CO_2 Separation in an Ultra-microporous Metal-Organic Framework via Copper(I)-Alkynyl Chemistry. *Angew. Chem., Int. Ed.* **2021**, *60*, 15995−16002.
(37) Zeng, H.; Xie, M.; Huang, Y.-L.; Zhao, Y.; Xie, X.-J.; Bai, J.-P.; Wan, M.-Y.; Krishna, R.; Lu, W.; Li, D. Induced Fit of C_2H_2 in a Flexible MOF through Cooperative Action of Open Metal Sites. *Angew. Chem., Int. Ed.* **2019**, *58*, 8515−8519.
(38) Zhang, Z.; Peh, S. B.; Wang, Y.; Kang, C.; Fan, W.; Zhao, D. Efficient Trapping of Trace Acetylene from Ethylene in an Ultramicroporous Metal-Organic Framework: Synergistic Effect of High-Density Open Metal and Electronegative Sites. *Angew. Chem., Int. Ed.* **2020**, *59*, 18927−18932.
(39) Xie, X.-J.; Zeng, H.; Xie, M.; Chen, W.; Hua, G.-F.; Lu, W.; Li, D. A Metal-Organic Framework for C_2H_2/CO_2 Separation under Highly Humid Conditions: Balanced Hydrophilicity/Hydrophobicity. *Chem. Eng. J.* **2021**, *427*, No. 132033.
(40) Bloch, E. D.; Queen, W. L.; Krishna, R.; Zadrozny, J. M.; Brown, C. M.; Long, J. R. Hydrocarbon Separations in a Metal-Organic Framework with Open Iron(II) Coordination Sites. *Science* **2012**, *335*, 1606−1610.
(41) Yang, S.; Ramirez-Cuesta, A. J.; Newby, R.; Garcia-Sakai, V.; Manuel, P.; Callear, S. K.; Campbell, S. I.; Tang, C. C.; Schröder, M. Supramolecular Binding and Separation of Hydrocarbons within a Functionalized Porous Metal-Organic Framework. *Nat. Chem.* **2015**, *7*, 121−129.
(42) Jiang, M.; Cui, X.; Yang, L.; Yang, Q.; Zhang, Z.; Yang, Y.; Xing, H. A Thermostable Anion-Pillared Metal-Organic Framework for C_2H_2/C_2H_4 and C_2H_2/CO_2 Separations. *Chem. Eng. J.* **2018**, *352*, 803−810.

https://doi.org/10.1021/acsami.2c09917
ACS Appl. Mater. Interfaces 2022, 14, 33429−33437

(43) Li, H.; Liu, C.; Chen, C.; Di, Z.; Yuan, D.; Pang, J.; Wei, W.; Wu, M.; Hong, M. An Unprecedented Pillar-Cage Fluorinated Hybrid Porous Framework with Highly Efficient Acetylene Storage and Separation. *Angew. Chem., Int. Ed.* **2021**, *60*, 7547−7552.
(44) Shivanna, M.; Otake, K.-I.; Song, B.-Q.; Van Wyk, L. M.; Yang, Q.-Y.; Kumar, N.; Feldmann, W. K.; Pham, T.; Suepaul, S.; Space, B.; Barbour, L. J.; Kitagawa, S.; Zaworotko, M. J. Benchmark Acetylene Binding Affinity and Separation through Induced Fit in a Flexible Hybrid Ultramicroporous Material. *Angew. Chem., Int. Ed.* **2021**, *60*, 20383−20390.
(45) Luo, F.; Yan, C.; Dang, L.; Krishna, R.; Zhou, W.; Wu, H.; Dong, X.; Han, Y.; Hu, T.-L.; O'Keeffe, M.; Wang, L.; Luo, M.; Lin, R.-B.; Chen, B. UTSA-74: A MOF-74 Isomer with Two Accessible Binding Sites Per Metal Center for Highly Selective Gas Separation. *J. Am. Chem. Soc.* **2016**, *138*, 5678−5684.
(46) Xue, Y.-Y.; Bai, X.-Y.; Zhang, J.; Wang, Y.; Li, S.-N.; Jiang, Y.-C.; Hu, M.-C.; Zhai, Q.-G. Precise Pore Space Partitions Combined with High-Density Hydrogen-Bonding Acceptors within Metal-Organic Frameworks for Highly Efficient Acetylene Storage and Separation. *Angew. Chem., Int. Ed.* **2021**, *60*, 10122−10128.
(47) Zhu, B.; Cao, J.-W.; Mukherjee, S.; Pham, T.; Zhang, T.; Wang, T.; Jiang, X.; Forrest, K. A.; Zaworotko, M. J.; Chen, K.-J. Pore Engineering for One-Step Ethylene Purification from a Three-Component Hydrocarbon Mixture. *J. Am. Chem. Soc.* **2021**, *143*, 1485−1492.

https://doi.org/10.1021/acsami.2c09917
ACS Appl. Mater. Interfaces 2022, 14, 33429−33437

Supporting Information

Two-Dimensional Metal-Organic Framework with Ultrahigh Water Stability for Separation of Acetylene from Carbon Dioxide and Ethylene

Shan-Qing Yang,[†] Lei Zhou,[†] Yabing He,[‡] Rajamani Krishna,[§] Qiang Zhang,[†] Yi-Feng An,[†] Bo Xing,[†] Ying-Hui Zhang,[†] Tong-Liang Hu*[†]

[†] School of Materials Science and Engineering, National Institute for Advanced Materials, Nankai University, Tianjin 300350, China. Email: tlhu@nankai.edu.cn (T.-L. Hu)

[‡] Key Laboratory of the Ministry of Education for Advanced Catalysis Materials, College of Chemistry and Life Sciences, Zhejiang Normal University, Jinhua 321004, China.

[§] Van 't Hoff Institute for Molecular Sciences, University of Amsterdam, Science Park 904, 1098 XH Amsterdam, The Netherlands.

Experimental Section

Breakthrough Simulations

The performance of industrial fixed bed adsorbers is dictated by a combination of adsorption selectivity and uptake capacity. Transient breakthrough simulations were carried out for the separation of C_2H_2/C_2H_4 (10/90 and 50/50, v/v), C_2H_2/CO_2 (50/50, v/v) and equimolar $C_2H_2/C_2H_4/CO_2$ mixtures in **NUM-11a** operating at a total pressure of 100 kPa, and temperature of 298 K, using the methodology described in earlier publications.[1-5] For the breakthrough simulations, the following parameter values were used: length of packed bed, $L = 0.3$ m; voidage of packed bed, $\varepsilon = 0.4$; superficial gas velocity at inlet, $u = 0.04$ m/s.

The *y*-axis is the dimensionless concentrations of each component at the exit of the fixed bed, normalized with respect to the inlet feed concentrations. The *x*-axis is the *dimensionless* time, $\tau = \frac{tu}{L\varepsilon}$, defined by dividing the actual time, *t*, by the characteristic time, $\frac{L\varepsilon}{u}$.

Notation

L length of packed bed adsorber, m

t time, s

T absolute temperature, K

u superficial gas velocity in packed bed, m s^{-1}

Greek letters

ε voidage of packed bed, dimensionless

τ time, dimensionless

Fitting of Pure Component Isotherms

The isotherm data for C_2H_2, C_2H_4 and CO_2 in **NUM-11a**, measured at 278, 288 and 298 K were fitted with the Dual-site Langmuir-Freundlich model.

$$q = q_{A,sat}\frac{b_A p^{c_A}}{1+b_A p^{c_A}} + q_{B,sat}\frac{b_B p^{c_B}}{1+b_B p^{c_B}}$$

Calculation for C_2H_2/C_2H_4 and C_2H_2/CO_2 Adsorption Selectivities

The ideal adsorbed solution theory (IAST) was used to estimate the composition of the adsorbed phase from the data of single component isotherms and predict the selectivities of binary mixtures C_2H_2/C_2H_4 and C_2H_2/CO_2.[6] IAST calculations of C_2H_2/C_2H_4 (1/99, 50/50, v/v,) and C_2H_2/CO_2 (50/50, v/v) mixtures adsorption at 278, 288, 298 K, respectively were performed by

$$S_{ads} = \frac{q_1/q_2}{p_1/p_2}.$$

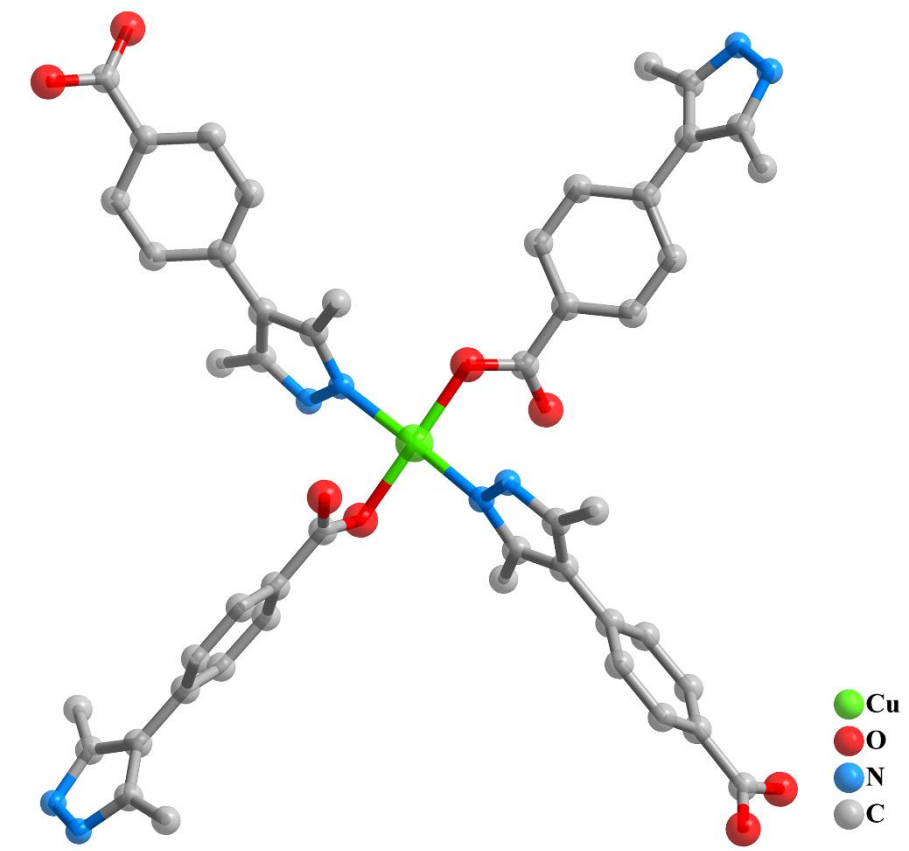

Figure S1. The coordination environment of the Cu^{2+}. (Hydrogen atoms and solvent molecules were omitted for clarity.)

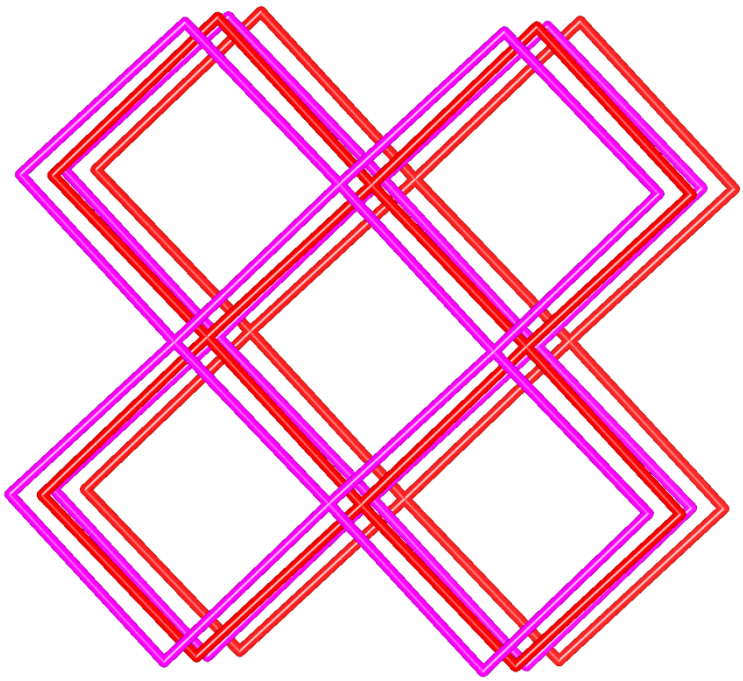

Figure S2. The *sql* topology for **NUM-11**.

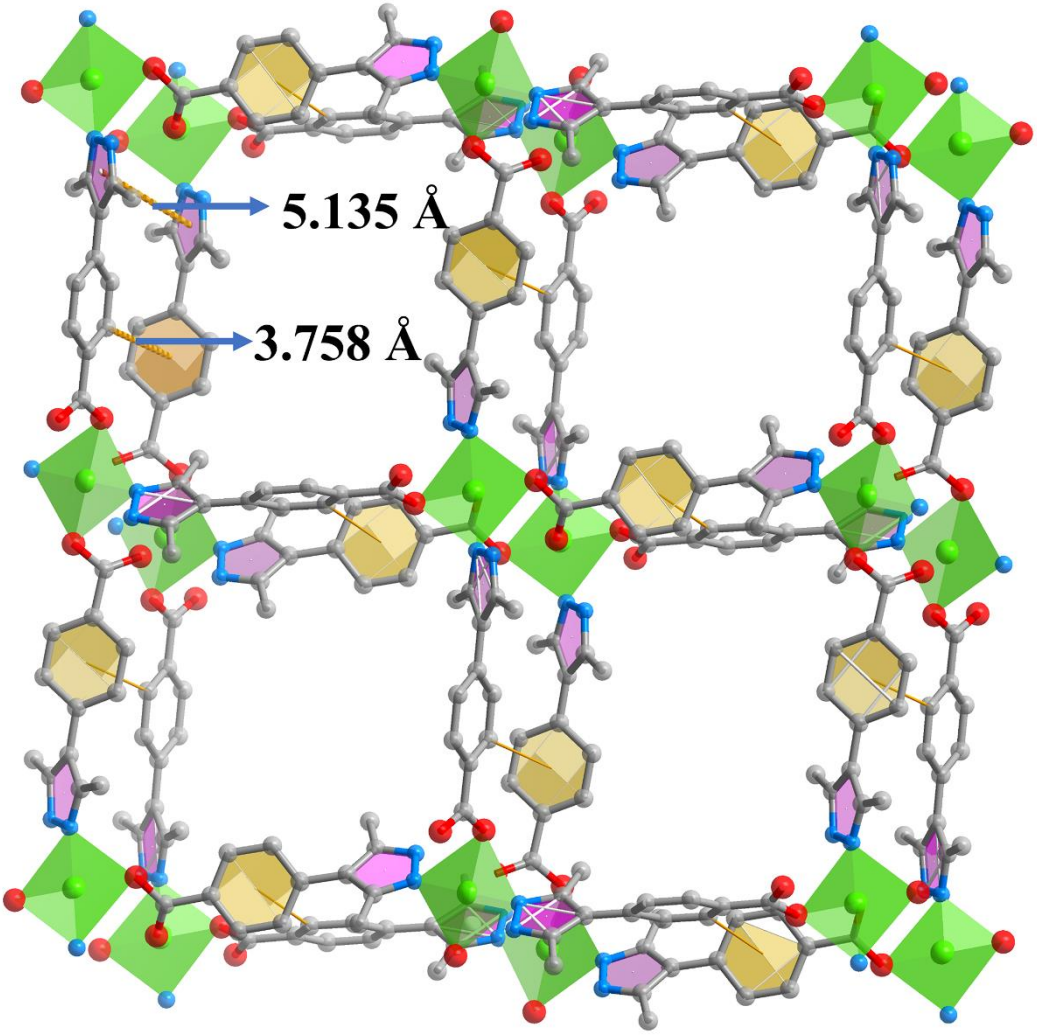

Figure S3. The 2D layers are stacked together through π-π interactions.

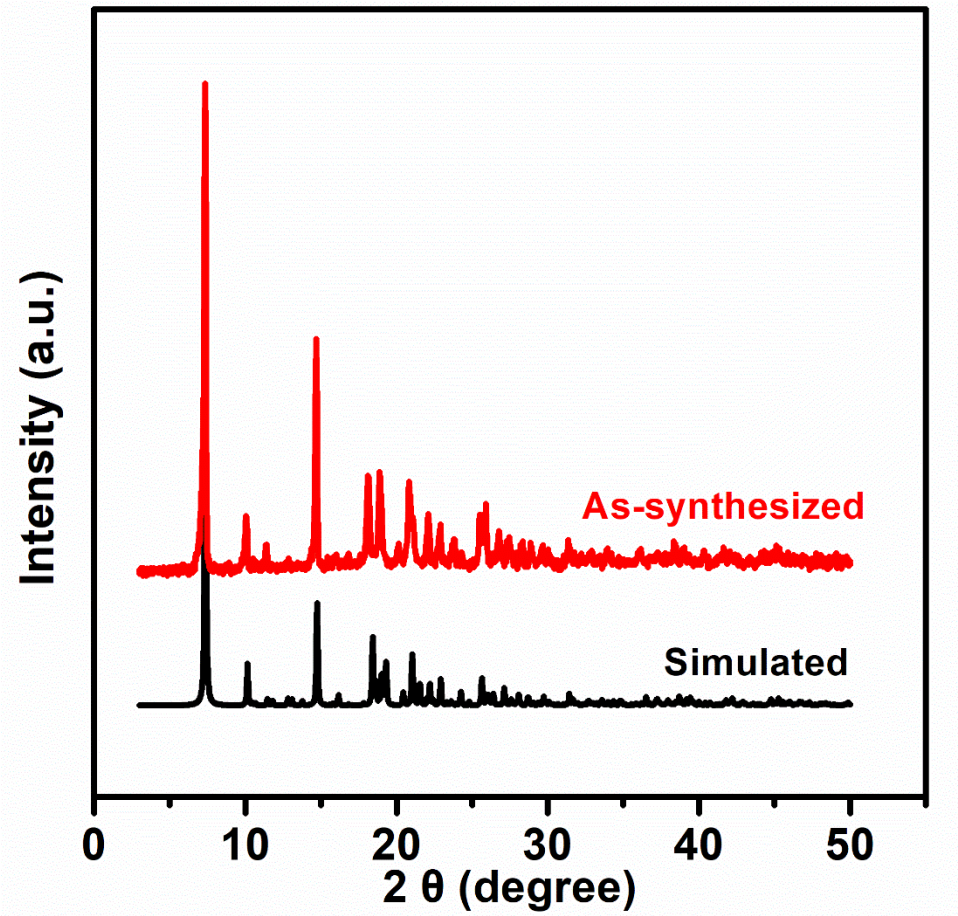

Figure S4. PXRD patterns of **NUM-11**. The experimental result of as-synthesized sample and the simulation one from single crystal X-ray diffraction data.

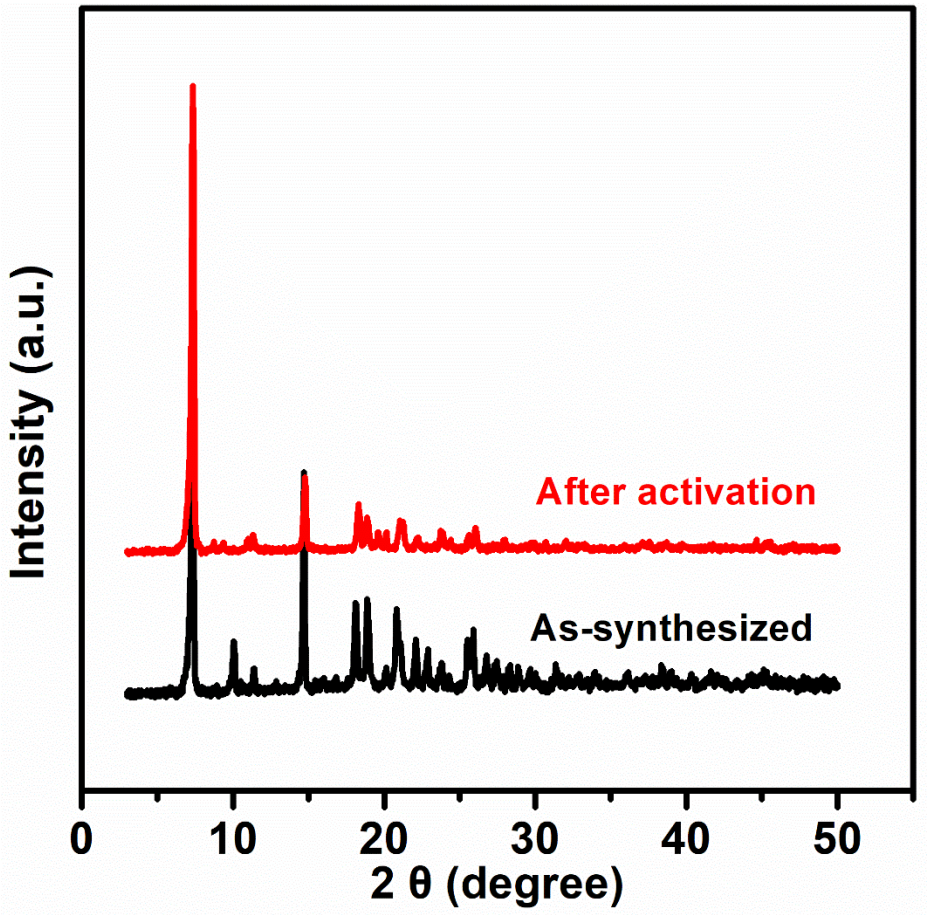

Figure S5. PXRD patterns of **NUM-11**. The experimental results of as-synthesized sample and the after-activation sample.

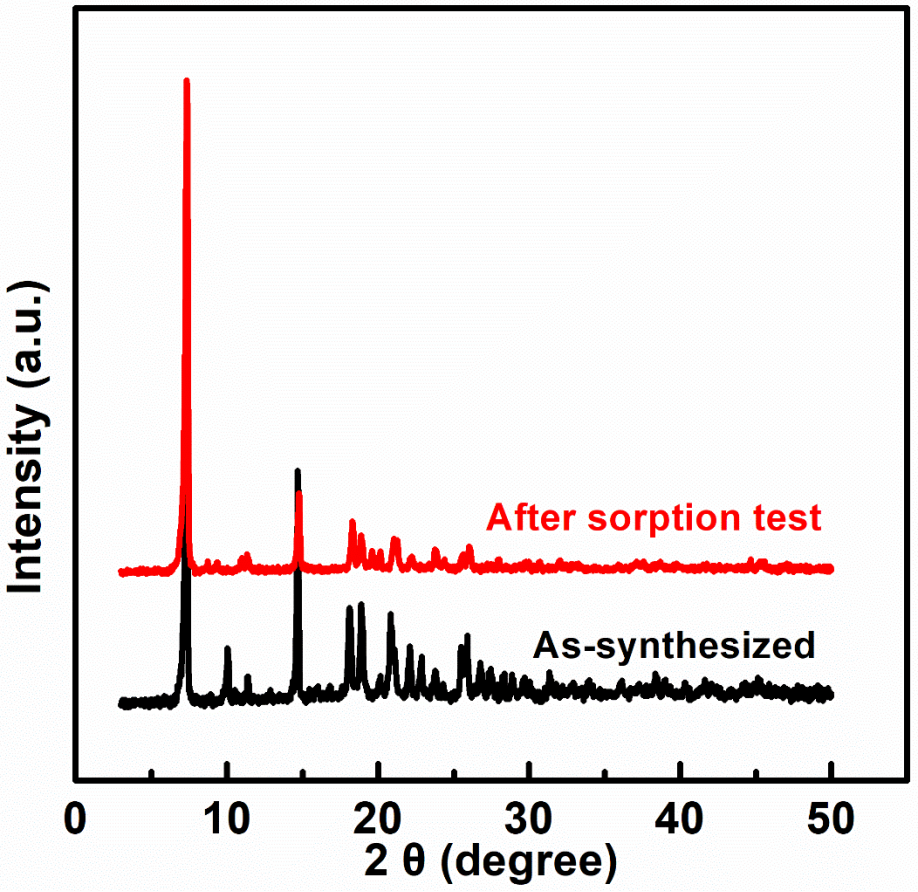

Figure S6. PXRD patterns of **NUM-11**. The experimental results of as-synthesized sample and the after sorption test.

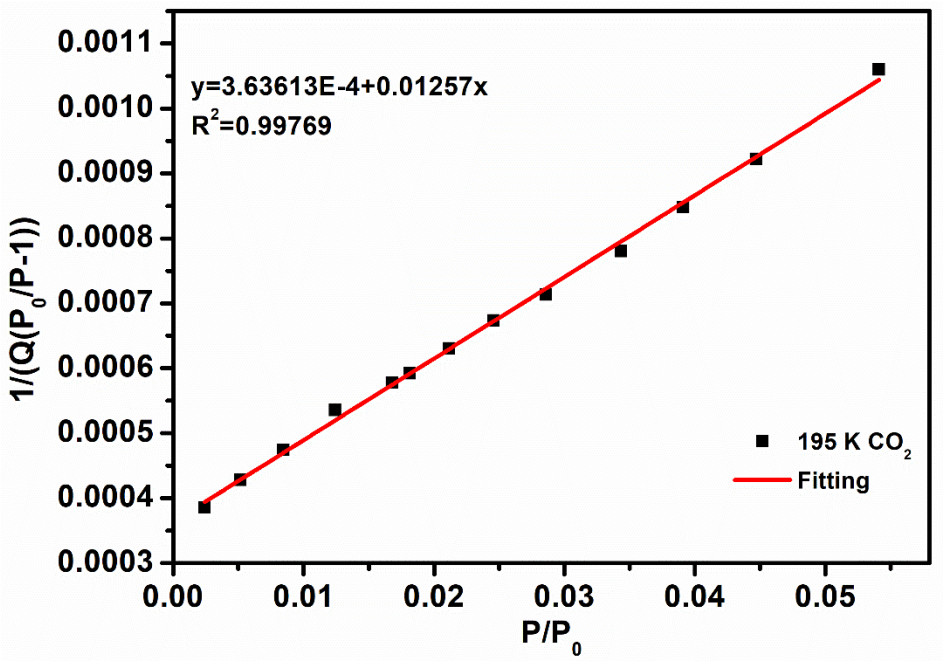

Figure S7. Calculation of BET surface area for **NUM-11a** based on CO_2 adsorption isotherm at 195 K.

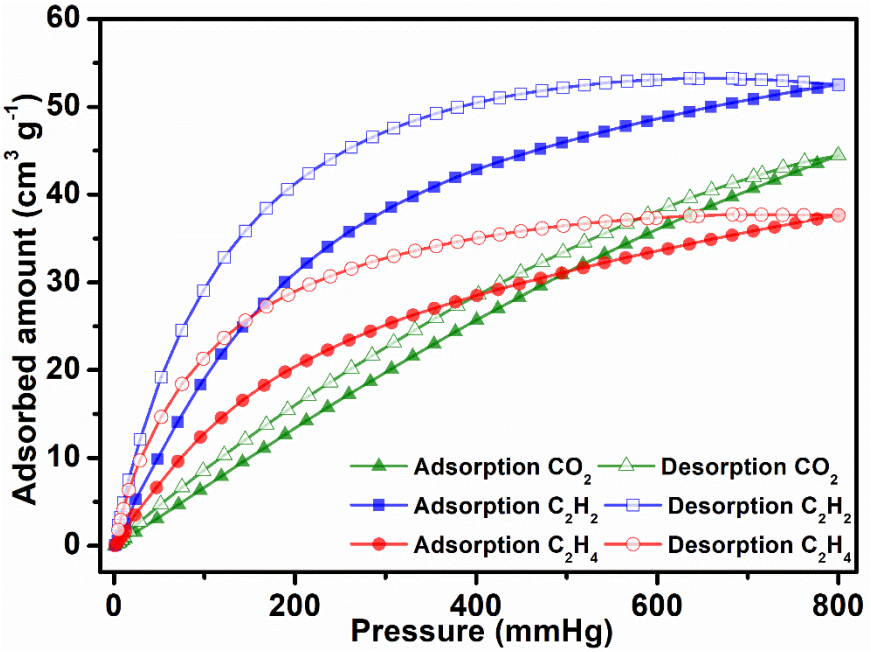

Figure S8. Single-component gas adsorption isotherms for C_2H_2 (blue), C_2H_4 (red), and CO_2 (green) at 278 K.

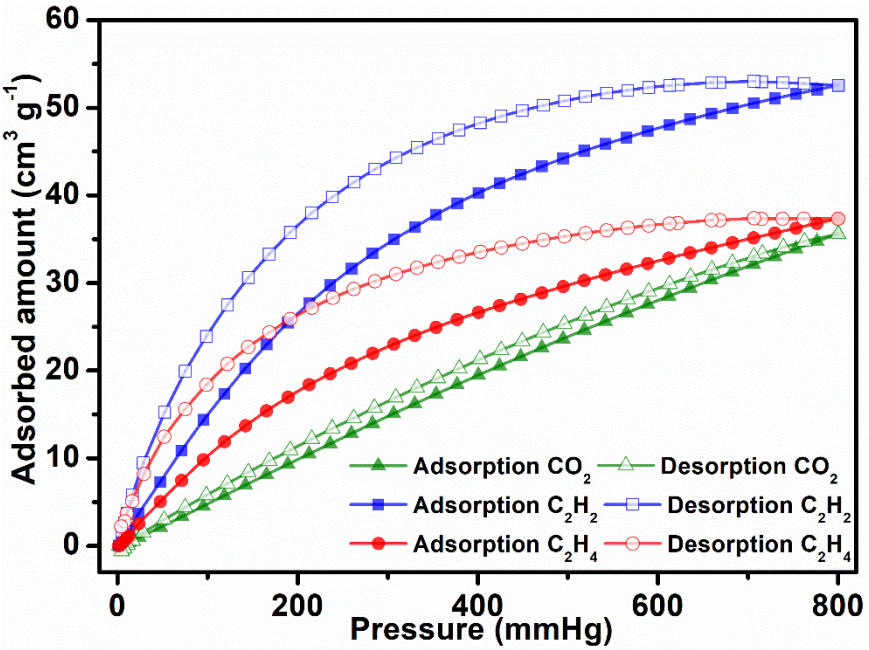

Figure S9. Single-component gas adsorption isotherms for C_2H_2 (blue), C_2H_4 (red), and CO_2 (green) at 288 K.

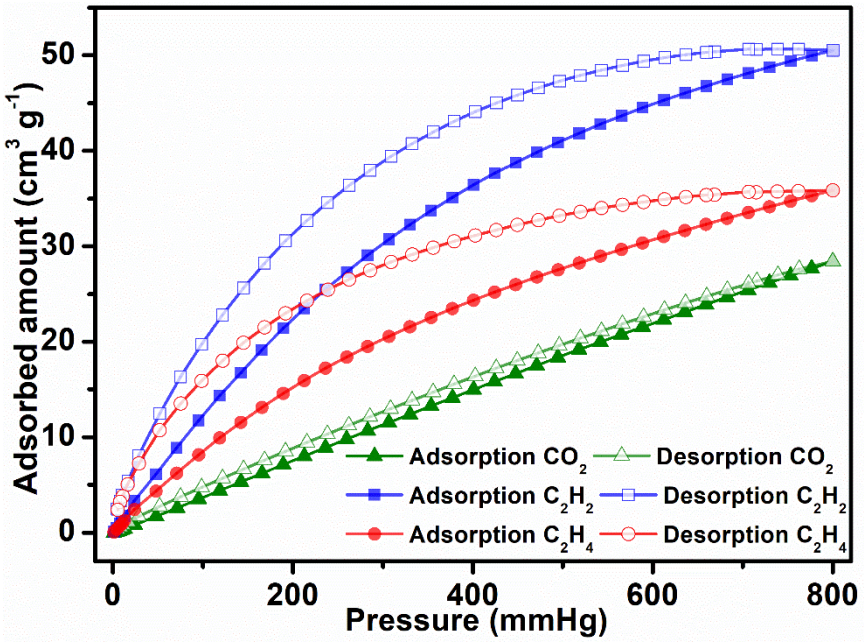

Figure S10. Single-component gas adsorption isotherms for C_2H_2 (blue), C_2H_4 (red), and CO_2 (green) at 298 K.

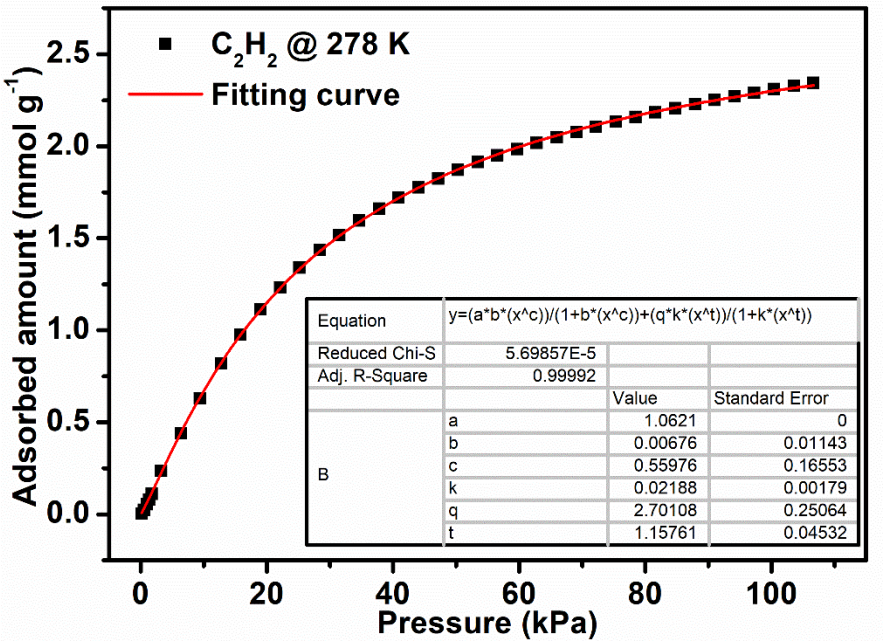

Figure S11. Dual-site Langmuir-Freundlich model for C_2H_2 adsorption isotherm on **NUM-11a** at 278 K.

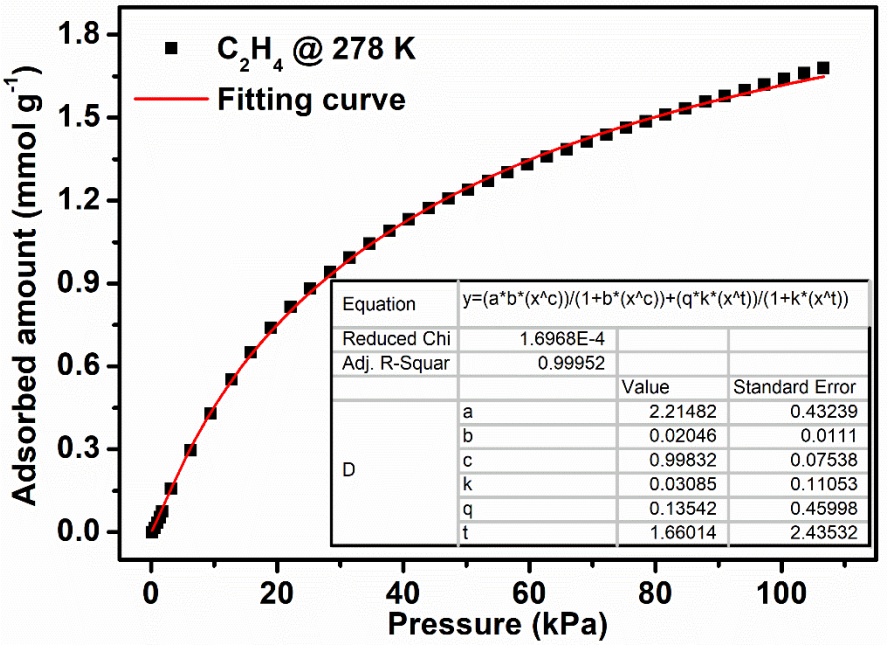

Figure S12. Dual-site Langmuir-Freundlich model for C_2H_4 adsorption isotherm on **NUM-11a** at 278 K.

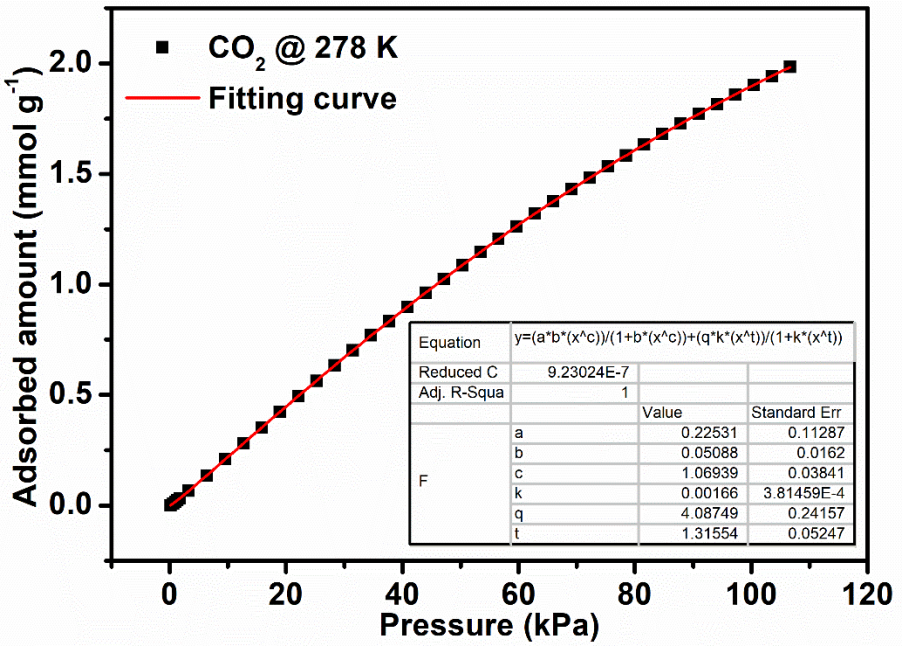

Figure S13. Dual-site Langmuir-Freundlich model for CO_2 adsorption isotherm on **NUM-11a** at 278 K.

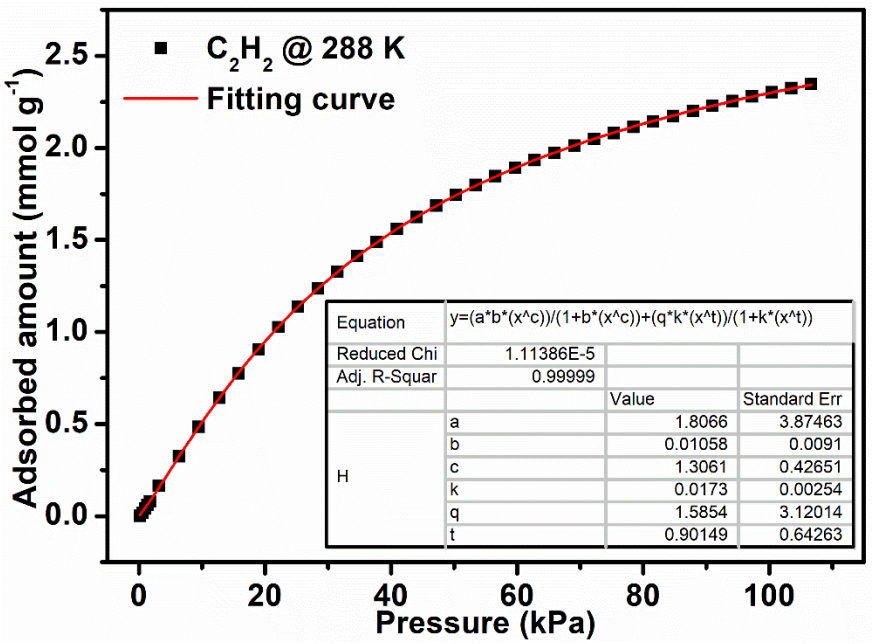

Figure S14. Dual-site Langmuir-Freundlich model for C_2H_2 adsorption isotherm on **NUM-11a** at 288 K.

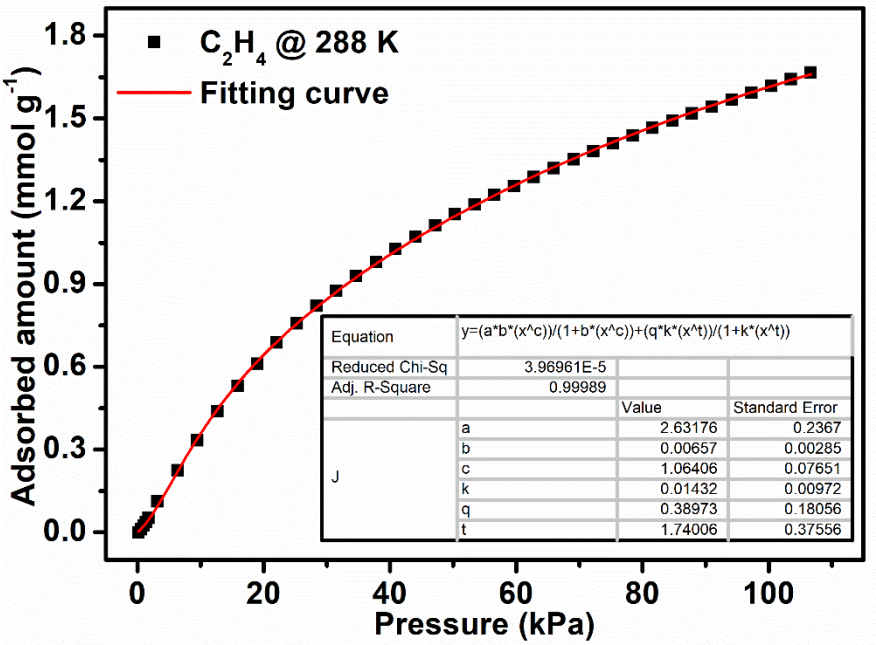

Figure S15. Dual-site Langmuir-Freundlich model for C_2H_4 adsorption isotherm on **NUM-11a** at 288 K.

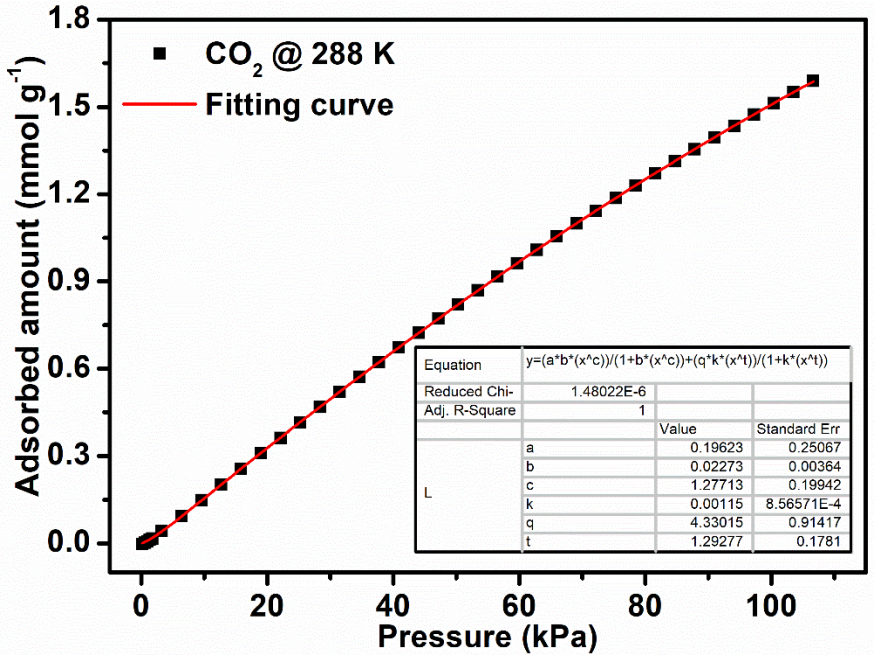

Figure S16. Dual-site Langmuir-Freundlich model for CO_2 adsorption isotherm on **NUM-11a** at 288 K.

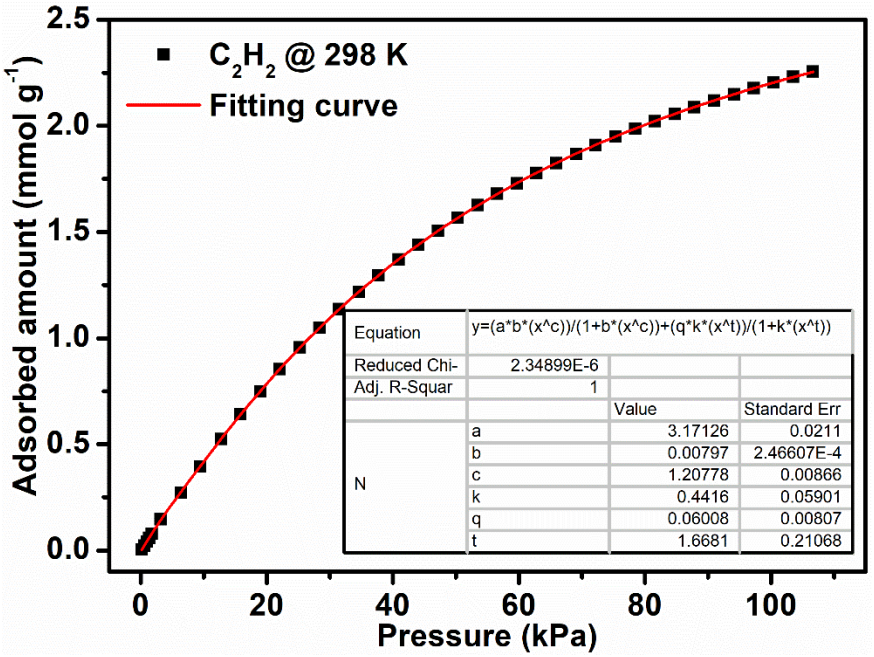

Figure S17. Dual-site Langmuir-Freundlich model for C_2H_2 adsorption isotherm on **NUM-11a** at 298 K.

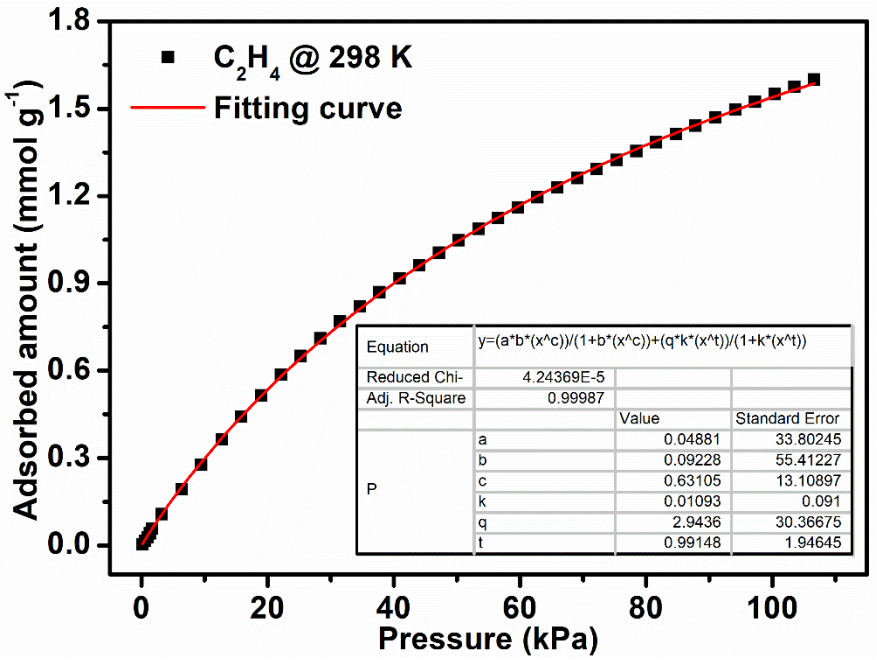

Figure S18. Dual-site Langmuir-Freundlich model for C_2H_4 adsorption isotherm on **NUM-11a** at 298 K.

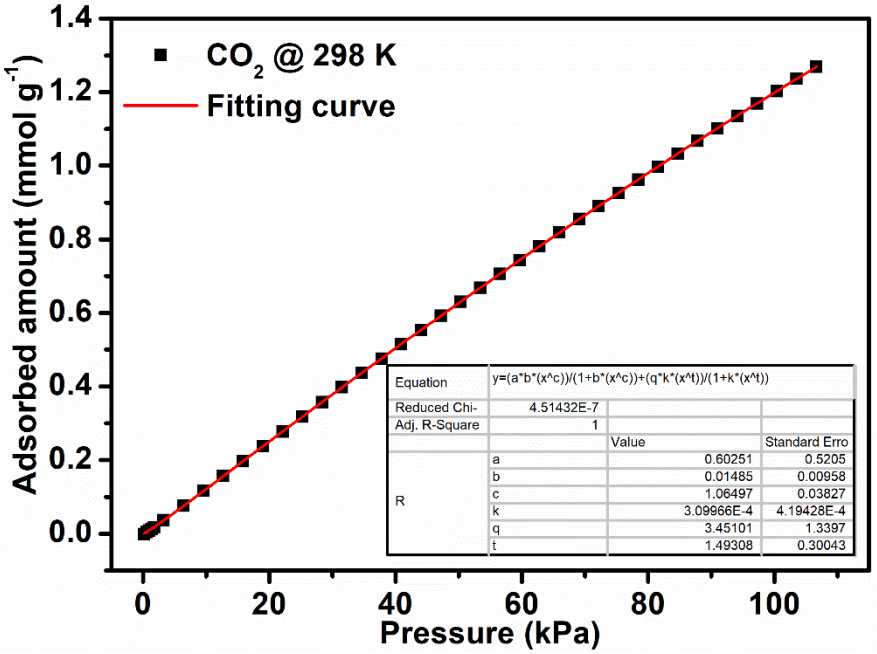

Figure S19. Dual-site Langmuir-Freundlich model for CO_2 adsorption isotherm on **NUM-11a** at 298 K.

References

(1) Krishna, R. The Maxwell-Stefan Description of Mixture Diffusion in Nanoporous Crystalline Materials, *Microporous Mesoporous Mater.* 2014, *185*, 30-50.

(2) Krishna, R. Methodologies for Evaluation of Metal-Organic Frameworks in Separation Applications, *RSC Adv*. 2015, *5*, 52269-52295.

(3) Krishna, R. Screening Metal-Organic Frameworks for Mixture Separations in Fixed-Bed Adsorbers Using a Combined Selectivity/Capacity Metric, *RSC Adv*. 2017, *7*, 35724-35737.

(4) Krishna, R. Methodologies for Screening and Selection of Crystalline Microporous Materials in Mixture Separations, *Sep. Purif. Technol.* 2018, *194*, 281-300.

(5) Krishna, R. Metrics for Evaluation and Screening of Metal-Organic Frameworks for Applications in Mixture Separations, *ACS Omega* 2020, *5*, 16987-17004.

(6) Myers, A. L.; Prausnitz, J. M. Thermodynamics of Mixed-Gas Adsorption. *AIChE J*. 1965, *11*, 121-127.